EXPERIMENTAL STUDY OF THE EFFECT OF
FORWARD SPEED AND HEEL ANGLE ON
LIFT ROLL DAMPING OF SMALL FISHING VESSELS

KIRK SING-KEUNG LEUNG

Experimental Study of the Effect of Forward Speed and Heel Angle on Lift Roll Damping of Small Fishing Vessels

by

©Kirk Sing-Keung Leung, B.Eng.

A thesis submitted to the School of Graduate

Studies in partial fulfilment of the

requirements for the degree of

Master of Engineering

Faculty of Engineering and Applied Science

Memorial University of Newfoundland

July 1993

St. John's   Newfoundland   Canada

ABSTRACT

An experimental study was carried out to investigate the effect of forward speed and heel angle on the bare hull lift component of roll damping. The effect of the presence of a rudder was also studied. Experiments were performed on two ship models with different hull characteristics. One of the models was also tested fitted with a rudder to investigate the effect of the rudder. The experiments were conducted in calm water with the ship model restrained from moving freely in any of the six directions. Models were oriented in different combinations of fixed heel angles and yaw angles, and towed at various forward speeds. The lift force and moment acting on the ship hull were measured and the lift coefficient and moment arm were calculated.

Experimental results show that the lift coefficient is a nonlinear function of the angle of attack. It is also dependent on heel angle and forward speed. The moment arm was found to be a nonlinear function of both heel angle and forward speed. Its value decreases as heel angle increases. An empirical formula was derived from the experimental results to determine the equivalent linear damping coefficient for lift roll damping. The empirical formula shows that the equivalent linear damping coefficient is a nonlinear function of forward speed. The lift roll damping will increase with increasing forward speed. On the other hand, increasing heel angle leads to a decrease in the value of the equivalent linear damping. Comparison between the empirical

formula and Ikeda's formula indicates that Ikeda's formula underestimates the equivalent linear damping. The discrepancy increases with increasing forward speed. Effect of the presence of a rudder is significant only at low speeds.

Neither Ikeda's formula nor the experimental results consider the sinkage of the ship while moving. This may be covered in future work.

ACKNOWLEDGEMENTS

CONTENTS

LIST OF FIGURES

LIST OF TABLES

LIST OF SYMBOLS

a	aspect ratio
t	time
L	length of waterline
B	beam at the waterline
T	draft
C_M	midship section coefficient
C_B	block coefficient
V	forward speed
Fn	Froude number
l_o	lever arm from roll axis to the point at which the angle of attack is measured
l_r	lift moment arm about roll/heel axis
L_o	vertical distance from linear strain gages to heel axis
OG	distance from still water level to roll axis
OG_o	OG value at zero forward speed
C_L	lift coefficient
k_N	slope of lift coefficient
β	coefficient in lift coefficient equation
n	exponent in lift coefficient equation

R	roll motion amplitude
F_e	measured force
F	lift force
M	measured lift moment
M_L	lift roll damping moment
B_e	equivalent linear damping coefficient
B_L	equivalent linear damping coefficient for lift roll damping
ρ	water density
ω	natural frequency
ψ	angle of attack/yaw angle
φ	roll/heel angle
$\dot{\varphi}$	roll velocity
$\ddot{\varphi}$	roll acceleration
$N(\varphi,\dot{\varphi})$	damping moment per unit virtual mass moment of inertia
$D(\varphi,t)$	restoring moment per unit virtual mass moment of inertia
$E(\varphi,t)$	excitation moment per unit virtual mass moment of inertia
ζ_1,ζ_2	non-dimensional linear damping coefficients
$\epsilon_1,\epsilon_2,\epsilon_3,\epsilon_4$	coefficients of nonlinear damping terms
a_0,a_1,b_0,b_1	regression coefficients
X_i,Y_i,x_i,y_i,p_i,q_i $(i=0,1,2)$	regression coefficients

CHAPTER 1   INTRODUCTION

Understanding ship motions in a seaway is important for good manoeuvrability and ship safety. Among all ship motions, rolling is one of the most complicated motions to predict. For accurate predictions of ship's roll response, good estimates of roll damping moment are crucial.

The nonlinear characteristics of roll damping caused by fluid viscosity, in addition to its strong dependence on the forward speed, make it difficult to predict the parameters of roll damping of ships. Moreover, the fact that these effects are of the same order of magnitude for ships without bilge keels further complicates the problem. The fact that empirical results obtained in the 1950's and 1960's by Hishida, Yamanouchi, Watanabe and Inoue (as reported by Himeno [1981]) are still often used and referred to, shows the difficulty and lack of analytical methods for the prediction of roll damping moment. Hence recourse to the use of empirical techniques is necessary.

Currently, two methods are available for the empirical prediction of roll damping moment. The first one uses either free or forced roll tests to measure the damping moment of a scaled model. The second method makes use of the empirical formulae available in the literature. Both methods have their own shortcomings.

1

In the past two decades, researchers focused on the study of hydrodynamic forces and moments acting on conventional lifting surfaces such as rudders, while the contribution from the bare hull as a lifting surface was ignored. The hydrodynamic forces and moments generated by the naked hull lift mechanism is generally expected to be much smaller than that generated by the rudder because of the poor section shape of ship hull as a lifting surface and its extremely low aspect ratio. However, one may refer to Crane et al. [1989], "… because of its very large profile area, a ship's hull does in fact generate forces and moments far larger than the control forces and moments generated by its rudder", to show that this is not the case. Moreover, a well known method of roll damping estimation by Ikeda et al. [1978] included bare hull lift damping as one of the five components of roll damping for a ship hull. As the forward velocity of the ship increases, the lift component is expected to be the most dominant ingredient of the roll damping moment. Hence for better estimation of the roll damping moment, further study of the lift component is necessary.

The objective of this work was to investigate experimentally the effect of forward speed and heel angle on the lift component of roll damping. Nevertheless, this is only a preliminary study of the lift roll damping. The experiments were only conducted in calm water with the ship model restrained from moving freely in any of the six directions. The next step would be repeating the same experiments with the model free

2

to heave and pitch. This may have effects on the values for lift obtained for the model in the heeled position while no effect is expected for the model in the upright condition.

In Chapter 2, Ikeda's method and previous research on the relationships among heel angle, forward speed and roll damping moments are reviewed. The experimental study method is presented in Chapter 3. The results from the experiments are analyzed and the equivalent linear damping coefficient is determined in Chapter 4. In Chapter 5, the calculated damping coefficient is compared to the results from Ikeda's method.

CHAPTER 2   BACKGROUND

Although roll motion should be considered as a coupled-three-degree-of-freedom problem involving sway and yaw motions, it is generally dealt with as a single-degree-of-freedom problem for the sake of simplicity. The equation of uncoupled rolling motion can be expressed as a simple single-degree-of-freedom form:

$$\ddot{\varphi} + N(\varphi,\dot{\varphi}) + D(\varphi,t) = E(\varphi,t) \tag{1}$$

where φ is the roll angle,
           $\dot{\varphi}$ is the derivative of φ with respect to time,
           $N(\varphi,\dot{\varphi})$ is the damping moment per unit virtual mass moment of inertia of the ship,
           $D(\varphi,t)$ is the restoring moment per unit virtual mass moment of inertia of the ship,
           $E(\varphi,t)$ is the excitation moment per unit virtual mass moment of inertia of the ship.

The damping term is usually expressed in terms of equivalent linear damping coefficient, B_e, as

$$N(\varphi,\dot{\varphi}) = B_e\dot{\varphi} \tag{2}$$

2.1 Roll Damping Dependence on Roll Angle

The conventional form of roll damping is the linear plus quadratic roll velocity dependent form devised by Froude [Haddara, 1984]. Recently, some other forms of damping moment were presented. They included use of a cubic term replacing the quadratic one, and the introduction of the dependence of damping moment on roll angle [Haddara, 1984].

The dependence of the damping moment on the roll angle was considered by Kerwin [1955] and Abicht [1975]. Kerwin assumed a linear dependence on the roll angle while Abicht assumed a quadratic dependence. In 1982, Cardo et. al. [1982] further investigated this roll angle dependence of the damping moment. They considered two generalized models. The first assumes a mixed linear dependence on the roll angle and linear-quadratic dependence on the roll velocity. The second assumes a mixed 'quadratic' with respect to φ and 'linear-cubic' with respect to $\dot{\varphi}$ model. These two models can be expressed as follows:

$$N(\varphi,\dot{\varphi}) = 2\zeta_1 \omega (\dot{\varphi} + \epsilon_1 |\varphi| \dot{\varphi} + \epsilon_2 |\dot{\varphi}| \dot{\varphi}) \tag{3}$$

$$N(\varphi,\dot{\varphi}) = 2\zeta_2 \omega (\dot{\varphi} + \epsilon_3 \varphi^2 \dot{\varphi} + \epsilon_4 \dot{\varphi}^3) \tag{4}$$

where ω is the natural frequency of the linear rolling motion,
       ζ_1, ζ_2 are the non-dimensional linear damping coefficients,
       $\epsilon_1, \epsilon_2, \epsilon_3, \epsilon_4$ are the coefficients of the nonlinear damping terms.

Cardo et. al. [1982] found that the curves of the decay of the free rolling oscillations obtained from these two damping models can equally well fit the experimental data obtained by Kerwin in 1955. However, they also concluded that the two models lead to different expressions for the maximum roll amplitude in regular waves, which in turn lead to different forecasts for forced rolling motion with the same excitation intensity.

In 1984, Haddara [1984] investigated the effect of the damping moment form, which included the above two damping models, on the rolling response of the ship. The results indicated that within the range and scatter of available data in the literature, all damping models were considered to represent equally well the rolling response with an appropriate choice of coefficients. However, for forced motion prediction, different damping models still lead to different motion response prediction outside their range of validity. Haddara [1984] suggested that this indicates the increased importance of rolling angle dependence of the damping moment as the angle increases.

Recently, Haddara and Bennett [1989] performed a study on the angle dependence of roll damping moment. By applying the Energy method, they showed that the damping moment - heel angle relationship may take a linear, a quadratic or a general nonlinear form. In addition, their tests with forward speed on an icebreaker model without bilge keels displayed little or no angle dependence of the damping moment at slower speed

6

while stronger angle dependence was noticed at higher speed. In contrast, the test results with bilge keels showed stronger angle dependence at lower speed than higher speed. All these previous studies showed the dependence of the damping moment on the rolling angle.

2.2   Forward Speed Dependence of Roll Damping

It is also known that roll damping is strongly dependent on forward speed. Watanabe [1977] stated that forward velocity affects the damping component rather than the inertial component of the hydrodynamic force. Troesch [1981] suggested that this dependence may be at least as important as the viscous damping. Indeed, this strong dependence is one of the reasons why prediction of roll damping is so difficult.

Past experimental results showed that the damping coefficient is linearly dependent on forward velocity, as reported by Haddara [1984]. However, results of stillwater roll decay tests with forward speed on an icebreaker model by Haddara and Bennett [1989] indicated that the equivalent linear damping coefficient increased in a nonlinear form with increasing forward speed.

Recently, Cumming, Haddara and Graham [1990] conducted an experiment on a destroyer model at a wide range of forward speeds to investigate the roll damping characteristics. They also observed a nonlinear dependence of the nonviscous damping component on the forward speed. The nonlinear function is generally quadratic in nature.

2.3   Lift Roll Damping

In 1978, Ikeda et. al. proposed a method for roll damping estimation. The method assumed that roll damping for a ship hull consists of five components. These are friction damping, eddy damping, wave damping, naked hull lift damping and bilge keel damping. Each component is determined by a different empirical formula.

When dealing with the lift damping component, Ikeda et. al. [1978] assumed that the hull can be treated as a flat plate having the same length and draft. The angle of attack ψ, is equal to the quantity of $\dot{\phi} l_o/V$, where l_o is the lever arm from the roll axis to the point at which the attack angle is measured and V is forward velocity. A semi-empirical expression for the slope of the lift coefficient with respect to the angle of attack, which is denoted by k_N, is taken as a function of the ship's length L, draft T, beam B and the midship section coefficient C_M, and is expressed as:

$$k_N = \frac{2 \pi T}{L} + \kappa \left(4.1 \frac{B}{L} - 0.045\right) \qquad (5)$$

$$where \quad \kappa = \begin{cases} 0, & C_M < 0.92 \\ 0.1, & 0.92 < C_M < 0.97 \\ 0.3, & 0.97 < C_H < 0.99 \end{cases}$$

The above expression seems to be an empirical modification of the Jones formula for a low aspect wing, which is described by Crane et. al. [1989] as follows:

$$\left(\frac{\partial C_L}{\partial \psi}\right)_h = \left(\frac{\pi}{2}\right)a, \quad per \ radian \qquad (6)$$

where C_L = lift coefficient,
          ψ = angle of attack,
          a = effective aspect ratio.

The modification includes the addition of a function in both the beam length ratio and the midship section coefficient, and the usage of an effective aspect ratio of (4T/L) for the hull. Equation (6) reflects that a thicker wing has higher slope for the lift curve. This function also assumes that the lift coefficient is independent of forward speed and of roll angle, and is a linear function of the angle of attack.

The equivalent linear damping coefficient due to the lift force was described by Ikeda et. al. [1978] as:

$$B_L = \frac{1}{2}\rho LTVk_N l_o l_r \qquad (7)$$

where L and T are the length and draft of the vessel, respectively. l_r represents the distance from the roll axis to the center of lift force on the hull. With the modification of the Yumuro's formula, the final prediction formula of the lift component was deduced in terms of equivalent linear damping as:

$$B_L = \frac{1}{2}\rho LTVk_N l_o l_r \left(1 - 1.4\frac{OG}{l_r} + \frac{0.7OG^2}{l_o l_r} \right) \qquad (8)$$

where   OG = distance from still water level to roll axis,
                  $l_o = 0.3T$,
                  $l_r = 0.5T$.

This final prediction formula implies that lift damping is linear and that its coefficient is proportional to forward speed. Moreover, the moment lever arm about the roll axis is assumed to be independent of forward velocity and of roll angle.

Schmitke [1978] stated in his paper that failure to include the effects of dynamic lift on a ship hull's lifting surface is one of the reasons for the failure to make accurate estimates of roll damping with forward speed. He included hull appendages such as the rudder, skeg and propeller shaft brackets as lifting surfaces in his work. However, he did not consider the bare hull as a lifting surface because of its poor section shape.

CHAPTER 3   EXPERIMENTAL STUDY

Towing tests were conducted on two ship models in the wave tank of the Faculty of Engineering and Applied Science, Memorial University of Newfoundland. The tank has the dimensions of 58.27 meters in length, 4.57 meters in width and 3.00 meters in depth. However, the tests were performed at a water depth of approximately 1.9 meters. The towing carriage has a capability of running from 0 to 5 meters per second in forward direction and 0 to 3 meters per second in reverse. The purpose of these tests was to measure the lift force and moment acting on a yawed ship travelling with forward speed. Hence the lift coefficient and the lift moment arm can be estimated.

Ship models were towed along the wave tank in calm water by the carriage at various forward speeds. In addition, the ship models were oriented in different combinations of fixed heel angles and yaw angles. Five fixed heel angles ranging from 0 to 20 degrees with a 5 degree increment and three yaw angles of 0, 3 and 6 degrees were used. The forward speeds ranged from 0.8 to 2.0 meters per second. The initial load due to the connection of the ship model to the frame for each combination was also recorded. Force and moment values were measured by strain gages mounted on two measuring elements. Models were fixed to the carriage so that they were restrained from moving freely in any of the six directions.

11

3.1 Strain Gages and Measuring Elements

Four sets of strain gages were used in the experiment. They were mounted on two measuring elements. Each measuring element contained one set of gages to measure transverse force and another set for the measurement of bending moment. Each set consisted of four strain gages which were connected to form a complete Wheatstone bridge.

The measuring elements were custom made by the Technical Services of Memorial University of Newfoundland. They were shaped, as shown in figure 1, to intensify the sensitivity of the strain gages while maintaining their rigidity.

3.2 Equipment Arrangement

One of the measuring elements was located at mid length of the model while the other was 20 centimeters behind it along the line of motion. The measuring elements rested on an exchangeable yaw plate that was connected to the bottom mounting plate, which was fixed to the model, by four threaded rods. Three yaw plates were prepared for the three different yaw angles used in the experiment. Exchangeable heel plates were used to connect the measuring elements to the yaw plate. Five sets of heel plates were

Bending Moment Strain Gages

Shear Force Strain Gages

Front View   Side View
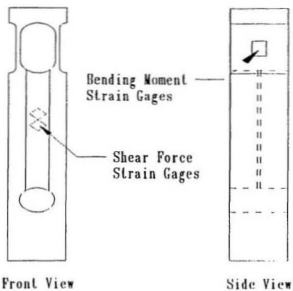
Figure 1   Measuring element

made for five different heel angles. The other end of the measuring elements were connected to two rigid frames which were fixed to the towing carriage by C-clamps. System S575 was used for the signal processing. Figure 2 is a schematic diagram of the equipment arrangement.
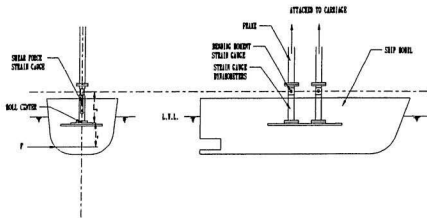
Figure 2   Equipment arrangement

3.3   Ship Models

Two ship models, designated M363 and M366, were used in the experiment. They were built by the Institute for Marine Dynamics (IMD). M363 is a 1:12 scale model of a small fishing vessel while M366 is a 1:6.8 scale model of another one. Both models have similar dimensions with water line length, beam and draft about 1.5 meters, 0.5 meters and 0.2 meters, respectively. However they have different hull characteristics. Model M363 represents the hard chine type while M366 is characterized

by a round bilge. Both models have no bilge keels but model M366 was also tested fitted with a rudder to investigate the effect of the rudder. The size of the rudder is 75 x 90 millimeters. M366R will designate model M366 fitted with a rudder. The particulars and the lines plans of the two models are presented in Table I, Figure 3 and Figure 4, respectively.

Table I. Model Particulars

Ship Model	M363	M366
Scale	1:12	1:6.8
Length (LWL), m.	1.551	1.590
Beam, m.	0.507	0.506
Draft, m.	0.221	0.205
L.C.B., m.	-0.109	-0.1375
Mass, Kg.	80.00	69.1
Period of Roll, Sec.	2.06	1.59
GM, m.	0.0549	0.0868
D/L	0.1425	0.129
B/L	0.327	0.318
C_M	0.746	0.612
OG, m.	0.041	0.028

Model M366R was fitted with a rudder having the dimensions 75 x 90 mm.
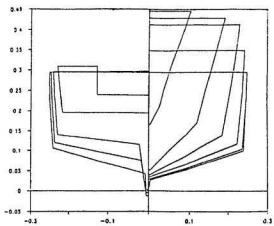
Figure 3   Lines plan of ship model M363
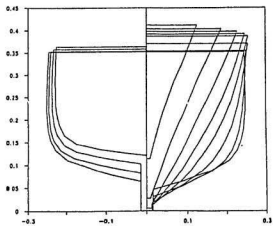
Figure 4   Lines plan of ship model M366

The ship models were ballasted to best suit the specifications sheet from the IMD while maintaining the shortest vertical distance possible between the heel axis and the center of gravity. The vertical position of the heel axis was obtained by measurement. Inclining tests were performed to determine the metacentric height, and hence the center of gravity. Heel axis was taken as the line passing through the center of the two heel plates along the top horizontal surfaces. Figure 5 shows the positions of the heel axis and center of gravity.

HEEL AXIS

HEEL PLATE

CENTER OF GRAVITY

G

K

NOT TO SCALE
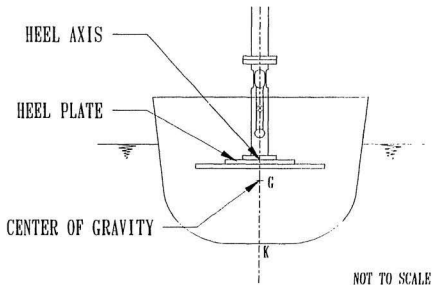
Figure 5   **Positions of heel axis and center of gravity**

The inclining test was repeated for various combinations of weight distribution and vertical heel axis position until the optimum result was reached. The center of

gravity was found to be 1.7 centimeters and 2.0 centimeters below the heel axis for model M363 and model M366, respectively.

3.4 Calibration

Calibration was done several times during the course of the experiment. The bending moment gages were calibrated to measure the bending moment at their location and the shear force gages were calibrated to record the force acting perpendicular to the measuring elements. The setup for calibration is shown in figure 6.

For experiments with the ship model in its upright position, the lift force was simply equal to the shear force recorded and the moment arm was obtained by dividing the measured bending moment by the shear force. For experiments with the ship model in a fixed heel angle and yaw angle, the measured force is:

$$F_s = F\cos\varphi\cos\psi \qquad (9)$$

where F_s = measured force,
           F = lift force acting on ship model,
           φ = fixed heel angle,
           ψ = fixed yaw angle.
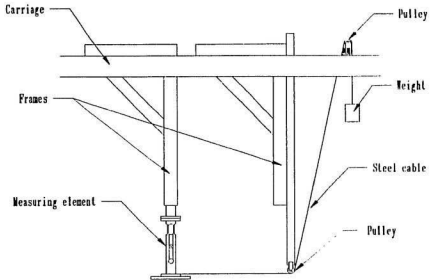
Figure 6   Calibration setup

Hence the lift force is:

$$F = \frac{F_x}{\cos\varphi\cos\psi} \qquad (10)$$

The relationship between the measured bending moment and lift moment arm is:

$$M = F\cos\psi\cos\varphi(L_0 + l_t\cos\varphi) + F\cos\psi\sin\varphi l_t\sin\varphi$$

$$= F\cos\psi L_0\cos\varphi + F\cos\psi l_t$$

$$= F\cos\psi(L_0\cos\varphi + l_t) \qquad (11)$$

where M = measured bending moment,
           L_0 = vertical distance from linear strain gages to heel axis,
           l_t = lift moment arm about the heel axis.

19

To calculate the lift moment arm l_r about the heel axis,

$$l_r = \frac{M}{F\cos\psi} - L_0\cos\varphi \qquad (12)$$

A free body diagram for the ship model in a fixed heel angle is presented in figure 7.
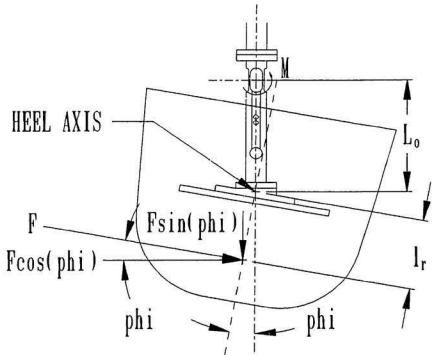

Figure 7   Free body diagram for the ship model in a fixed heel angle

CHAPTER 4   RESULTS AND ANALYSIS

The lift force can be expressed as

$$F = \frac{1}{2} \rho V^2 LTC_L \qquad (13)$$

where ρ is the water density, V is the model forward speed, L is the length of the water line of the model, T is the draft and C_L is the lift coefficient. The surface area of the ship hull as a lifting surface is assumed to be its length of waterline multiplied by its draft.

It is assumed that the lift coefficient measured for a ship hull towed at a constant yaw angle can be used to calculate the lift roll damping. In this study, the lift coefficient C_L is assumed to be a nonlinear function of the angle of yaw ψ. Hence, the lift coefficient can be expressed as

$$C_L = \psi^n \beta \qquad (14)$$

The value of β is also assumed to be dependent on both the forward velocity V of the model, and the heel angle φ.

When a ship is advancing at a constant speed and performing rolling motion at the same time, the hull is acting as a lifting surface whose angle of attack varies with the

vertical coordinate. However, it can be assumed that the lift force can be equivalently generated by a lifting surface located at an average distance l_r from the water line and having an average angle of attack given by

$$\psi = \frac{l_r \dot{\phi}}{V} \qquad (15)$$

One can then relate the measured lift force to the roll damping moment in this case.

Hence, equation (13) becomes

$$F = \frac{1}{2} \rho V^{(2-n)} L T \beta (l_r \dot{\phi})^n \qquad (16)$$

Using equation (16), an expression for the lift component of the roll damping moment can be written as

$$\begin{aligned} M_L &= F l_r \\ &= \frac{1}{2} \rho V^{(2-n)} L T \beta l_r^{(1+n)} \dot{\phi}^n \end{aligned} \qquad (17)$$

The lift roll damping moment can also be expressed in terms of the equivalent linear damping coefficient B_L as

$$M_L = B_L \dot{\phi} \qquad (18)$$

An expression for B_L can then be obtained by equating the integral of equations (17) and (18) over one quarter of the period of roll. Thus,

$$\int_0^R B_L \dot{\varphi} \, d\varphi = \int_0^R \frac{1}{2} \rho V^{(2-n)} L T \beta l_r^{(1+n)} \dot{\varphi}^n \, d\varphi \qquad (19)$$

The value of the lift force F was obtained directly from the experiment and the application of equation (10). The lift coefficient and the moment lever arm were then calculated from the lift force, the measured force and measured moment values. Equation (13) was used to determine the value of the lift coefficient. The point of application of the lift force was also found by using equation (12).

The values of the force and moment at non zero angles of yaw were obtained by subtracting the values measured for the model towed with zero angle of yaw from the corresponding value measured with the model towed obliquely. This was done to eliminate the effects due to the static heel. Similarly, the force and moment values at non zero forward speed were obtained by subtracting the values measured for the motionless model from the corresponding value measured with the model towed at constant forward speed. The purpose of this is to isolate the effect of forward speed from the stationary load due to the experimental setup.

The analysis has been carried out for the three ship models M363, M366 and M366R. The analysis of the effect of forward speed on lift roll damping for ship model in the upright condition will be presented first. This will be followed by the investigation of the additional effect caused by heel angles.

4.1 Ship Model in the Upright Condition

The values of the force and the moment were plotted against the Froude Number for each of the three ship models M363, M366 and M366R. The graphs are given in figures 8(a)-(c) and 9(a)-(c). Both force and moment values can be fitted to quadratic polynomials. The Least Square method was used for curve fitting throughout this study.

The value of the exponent n in equation (14) was determined by using regression analysis and found to be 0.6, 0.5 and 0.5 for M363, M366 and M366R, respectively. The values of the coefficient β were then calculated. They were plotted against the Froude Number and the results are shown in figures 10(a)-(c). These graphs show that the values of coefficient β for the M366 and M366R are almost constant until a value of Fn=0.35 is reached, after which the value of β starts increasing. For M363, β decreases slightly until a Froude Number of 0.35 is reached, then it starts increasing.
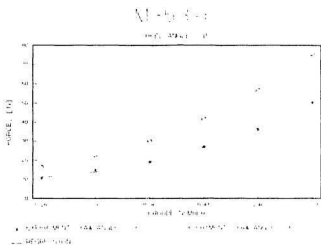
Figure 8(a)   Force vs. Fn for M363 in upright condition
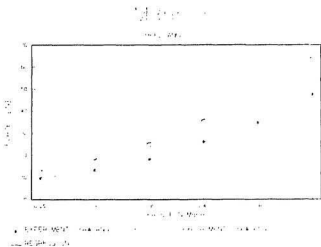


Figure 8(b)   Force vs. Fn for S366 in upright condition
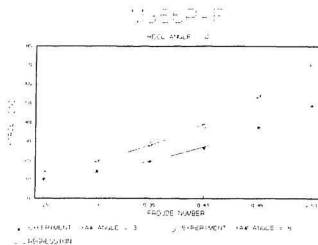
**Figure 8(c)   Force vs. Fn for M366R in upright condition**
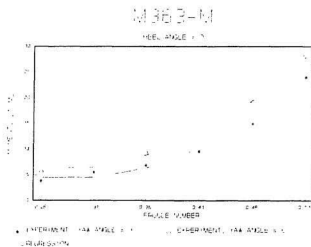
**Figure 9(a)   Moment vs. Fn For M363 in upright condition**
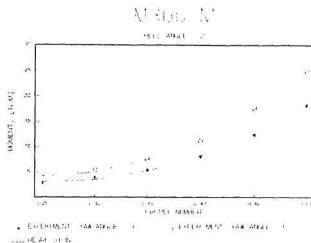
**Figure 9(b)   Moment vs. Fn for M366 in upright condition**
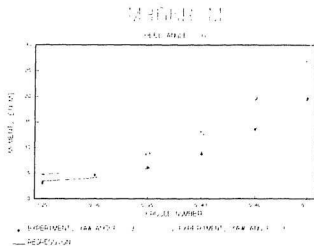
Figure 9(c)   Moment vs. Fn for M366R in upright condition

The value of β can be fitted to the following quadratic polynomial

$$\beta = X_0 + X_1 Fn + X_2 Fn^2 \qquad Fn \geq 0.25 \qquad (20)$$

The values of the coefficients X_0, X_1 and X_2 of the quadratic polynomial are presented in Table II.

The value of the coefficient β for M363 is found to be higher than that for the other two models. This ma_ .e explained by the fact that model M363 has higher values for the draft length ratio (T/L), the beam length ratio (B/L) and the mid-ship coefficient (C_M) than model M366. This leads to a higher aspect ratio and thickness ratio values for model M363 than that for model M366. Wings having higher aspect ratio are known to have higher lift-curves slopes which increase with increasing thickness ratio [Abbott and Von Doenhoff, 1959, p.6 and p.132]. This also agrees with Ikeda's equation for the slope of the lift curve, see equation (5). An increase of about 10% in the value of β due to the presence of a rudder can be seen from figures 10(b) and 10(c).

Table II. Quadratic Fit for β

| Coefficient	M363	M366	M366R
X_0	0.7053	0.3976	0.3709
X_1	-2.0651	-0.9875	-0.7553
X_2	2.9747	1.6107	1.3439
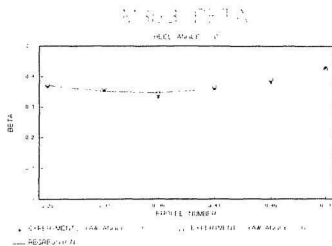
**Figure 10(a)** β vs. Fn for M363 in upright condition
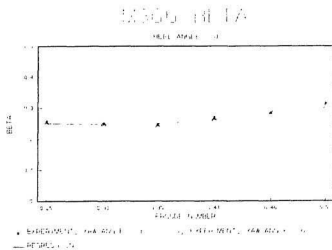
Figure 10(b) β vs. Fn for M366 in upright condition
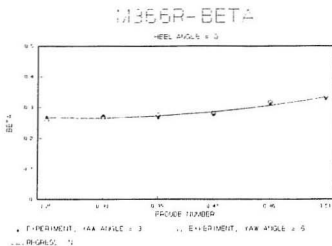
Figure 10(c) β vs. Fn for M366R in upright condition

The moment arm l_r about heel axis has also been computed for the three models. Figures 11(a)-(c) are plots of the non-dimensional moment arm l_r/T about heel axis against Froude Number for the three ship models. From the graphs, the moment arm about the heel axis seems to be a nonlinear function of the Froude Number. This function can be fitted to a quadratic polynomial which can be expressed as

$$\frac{l_r}{T} = Y_0 + Y_1 Fn + Y_2 Fn^2 \qquad Fn \geq 0.25 \qquad (21)$$

The coefficients Y_0, Y_1 and Y_2 of the polynomial are given in Table III. The values of l_r/T first declines slightly until a Froude Number of about 0.35 has been reached, then its value increases again in a nonlinear fashion. This may decipher the observation made

by Cumming, Haddara and Graham [1990] that some models will have a decreasing damping coefficient with the increase in forward speed until a certain value of Froude Number has been reached, then it increases again.
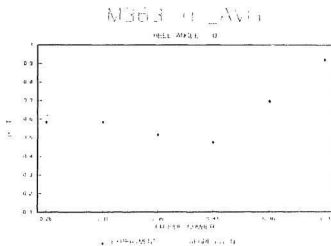
Figure 11(a) l_r/T vs. Fn for M363 in upright condition

In addition, the result that l_r is a function of forward speed shows that increasing forward velocity does not necessarily mean decreasing the angle of attack, which is indicated by equation (14). However, this point needs further study.

M363 has the largest value of moment arm about the heel axis among the three ship models in upright hull condition. The figures also demonstrate the effect of the rudder on the value of l_r/T. It is clearly shown in figures 11(b) and 11(c) that the rudder
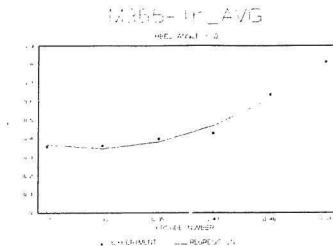
Figure 11(b) l_r/T vs. Fn for M366 in upright condition
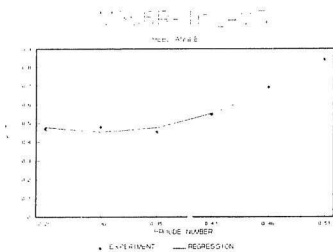
Figure 11(c) l_r/T vs. Fn for M366R in upright condition

Table III. Quadratic Fit for l_r/T

Coefficient	M363	M366	M366R
Y_0	2.3670	1.3004	1.3511
Y_1	-10.7637	-6.4177	-5.8979
Y_2	15.4349	10.7845	9.6855

has a greater effect at lower speed than higher speed, with the hull in upright condition. The increase in the l_r/T value due to the presence of the rudder changes from about 42% at a Froude Number of 0.25 to about 4% at a Froude Number of 0.51.

An expression for the equivalent linear damping coefficient of the ship model in the upright condition can be obtained by substituting φ with $R\sin(\omega t)$ into equation (19). Hence, the expression is given as

$$B_L = \frac{2\alpha}{\pi} \rho V^{(2-n)} L \, T l_r^{(1+n)} \beta (\omega R)^{(n-1)} \qquad (22)$$

where R is the roll amplitude and ω is the natural frequency of the ship model. α is given by

$$\alpha = \int_0^{\frac{\pi}{2}} \cos^{(1+n)} u \; du$$

The values of l_r and β can be obtained from equations (20) and (21), respectively.

33

The equivalent linear damping coefficient B_L has been computed for the three ship models in the upright condition. The results are presented in Figure 12. The graph clearly shows that B_L is a nonlinear function of the Froude Number for all three ship models. The value of B_L increases slightly for the range of $0.25 \leq \text{Fn} \leq 0.41$ and can be approximated as a linear function in Froude Number. However, there is a drastic increase in the slope of B_L as a function of Fn after the Froude Number has reached 0.41. This can be explained by the nonlinear behaviour of the moment arm about heel axis as a function in Froude Number. Moreover, the nonlinear dependence of B_L on l_r, as can be seen from equation (22), also contributes to the behaviour observed in Figure 12.

The effect of the rudder on the equivalent linear damping coefficient is also shown in Figure 12. The relative effect is more significant at low speed. At a Froude Number of 0.25, the presence of a rudder increases the value of B_L by 59%. The increase in the value of B_L caused by the rudder drops to about 13% only at a Froude Number of 0.51. At a reasonable Froude Number of 0.46 which corresponds to a speed of 9.5 knots for the full scale ship, the damping coefficient is increased by about 23% due to the presence of the rudder.

Model M363 has the highest value of the equivalent linear damping coefficient in the upright condition among the three ship models. This may be attributed to the hard

34
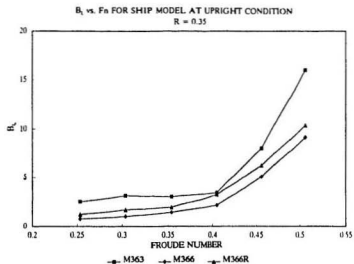
Figure 12 B_L vs. Fn for models M363, M366 and M366R in upright condition

chine characteristics of the ship hull. One should also investigate the effect of the rise of floor. Comparison of the damping coefficient with Ikeda's theory will be discussed in the next chapter.

4.2 Ship Model at a Constant Angle of Heel

4.2.1 Effect of Forward Speed

The values of force, moment, coefficient β and moment arm about heel axis were also plotted against the Froude Number for the four different fixed heel angles for each ship model. Graphs of lift force versus Froude Number and moment versus Froude Number are shown in Appendices A and B, respectively. Similar to the ship model in the upright condition, both force and moment values can be fitted to quadratic polynomials for all three ship models. It can be seen from the graphs that the force and moment values increase in a quadratic fashion as the forward speed increases. While there is no significant difference between the force values for models M363 and M366, the moment values for M363 is slightly higher than M366. This indicates that the moment arm value for M363 will probably be larger than that for M366. The effect of the presence of the rudder on the force and moment values cannot be generalized for the heeled model.

The values of the coefficient β were plotted against Froude Number for the four non-zero heel angles. The results are presented in Figures 13(a)-(d) for M366R while the results for M363 and M366 can be found in Appendix C. The same values of n as for the case of upright condition are found for the four different heel angles. The values

36

of coefficient β for the heeled models behave the same way as in upright condition. They can also be fitted to quadratic polynomials.
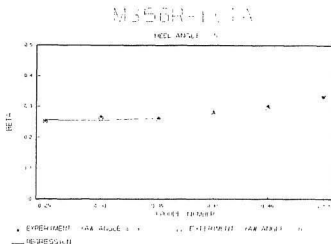
Figure 13(a) β vs. Fn for M366R at $\varphi = 5°$

For heel angles less than 10 degrees, values of β for M366R are slightly larger than M366 but vice versa for heel angles equal to or greater than 10 degrees. Generally, the rudder shows no significant effect on the value of the coefficient β.

The graphs of the non-dimensional moment arm l_r/T about the heel axis versus Froude Number for the four fixed heel angles are presented in Figures 14(a)-(d) for M366R. Graphs for the other two ship models are shown in Appendix D. Similar to the ship model in the upright condition, l_r/T is a nonlinear function of Froude Number.
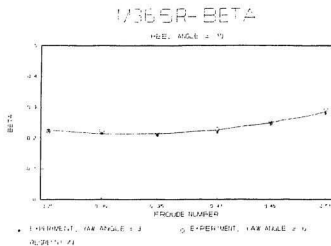
Figure 13(b) β **vs. Fn for M366R at** $\varphi = 10°$
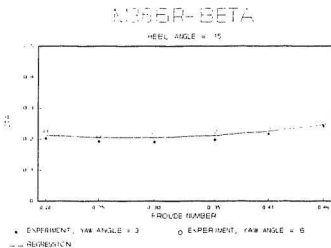
Figure 13(c) β **vs. Fn for M366R at** $\varphi = 15°$
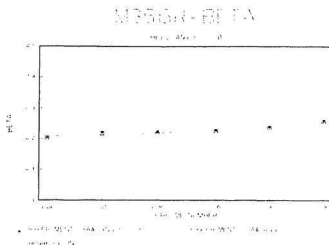
Figure 13(d) β vs. Fn for M366R at $\varphi = 20^\circ$

Except for the scattered values at heel angle equal to 15 degrees, the l_i/T values can generally be fitted to a quadratic polynomial. The effect of rudder on the moment arm about the heel axis cannot be generalized for non-zero heel angles from these figures.

4.2.2 Effect of Heel Angle

To investigate the effect of heel angle from another perspective, the values of the four parameters, force, moment, coefficient β and moment arm about the heel axis were plotted against heel angle for the five constant forward speeds.
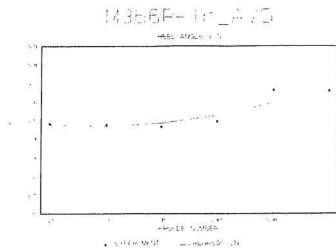
39

Figure 14(a) l_r/T vs. Fn for M366R at $\varphi = 5^o$
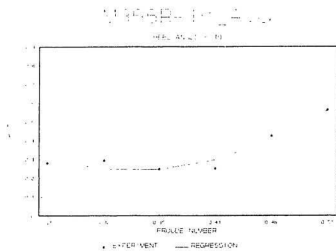
Figure 14(b) l_r/T vs. Fn for M366R at $\varphi = 10^o$
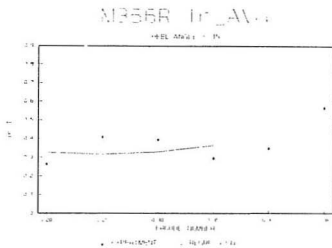
Figure 14(c) l_t/T vs. Fn for M366R at $\varphi = 15°$
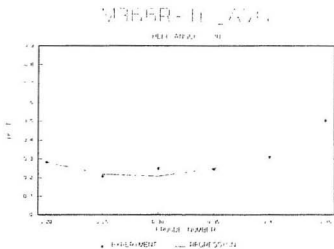
Figure 14(d) l_t/T vs. Fn for M366R at $\varphi = 20°$

The graphs of lift force versus heel angle and moment versus heel angle for the three ship models are presented in Appendices E and F, respectively. From the graphs, it can be seen that the moment values of all three ship models decrease in quadratic form as the heel angle increases. The decrease is gradual for M363 and M366R after the heel angle has reached 10 degrees. In fact, the moment values for M363 at 3 degrees yaw increase when the heel angle is greater than 1 degrees. This increase in the moment values is more evident as the forward speed goes up. The values of force for model M366R also decrease in a quadratic fashion for both yaw angles. However, the lift force values for M363 and M366 remain constant at a yaw angle of 3 degrees and appear as a nonlinear function of heel angle for a yaw angle of 6 degrees.

The values of β were also plotted against the heel angle as shown in Figures 15(a)-(e) for M366R. The graphs for models M363 and M366 can be seen in Appendix G. A linear plus quadratic model ($b_0 + b_1\varphi^2$) was chosen to fit the data. The values of β can be fitted by the model for all three ship models. The values of β for model M366R decrease slightly as the heel angle increases, while β seems to be insensitive to the change in heel angle for M363 and M366. Again, it can be seen from these graphs that the values of β are larger for M363 than M366 and M366R. As in the case of the upright condition, this may also be explained by the effect of higher aspect ratio and thickness ratio values for model M363 than that of model M366. The figures show that

these effects are independent of heel angle. This is because changes of heel angle do not vary the effective aspect ratio and thickness ratio.
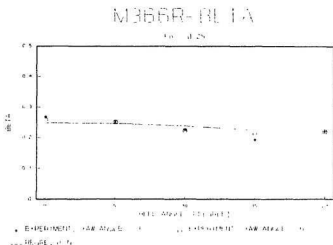
Figure 15(a) β vs. φ for M366R at Fn = 0.25

Figures 16 and 17 are graphs of non-dimensional values of moment arm, l_r/T, about the heel axis versus heel angle for M363 and M366. The graphs for model M366R are shown in Appendix H. The linear plus quadratic model $(a_0 + a_1\varphi^2)$ was again used to fit the data. The graphs show that the values of l_r/T decrease as the heel angle increases for all three ship models. This decrease of the l_r/T values is similar, in a qualitative sense, to the behaviour of the pressure center of a submerged inclined flat plate which is subjected to the hydrostatic force. It is known that the vertical distance from the water surface to the center of pressure of the inclined flat plate is affected by
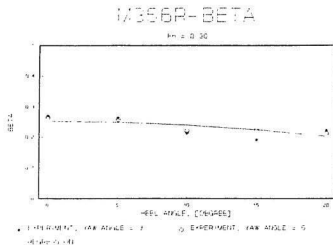
Figure 15(b) β vs. φ for M366R at Fn = 0.30
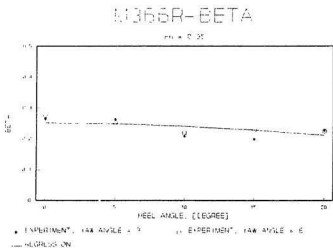
Figure 15(c) β vs. φ for M366R at Fn = 0.35
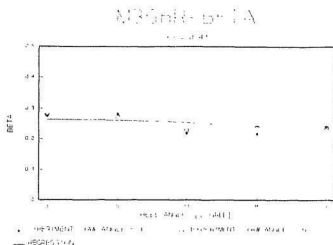
Figure 15(d) β vs. φ for M366R at Fn = 0.41
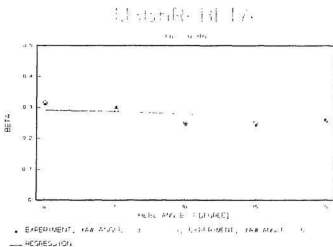
Figure 15(e) β vs. φ for M366R at Fn = 0.46

the incline angle. The incline angle is defined as the angle between the flat plate and the water surface. The distance will decrease with decreasing incline angle [White, 1986, p.67].
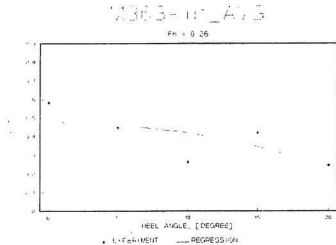
Figure 16(a) l_r/T vs. φ for M363 at Fn = 0.26

Two peculiar phenomena are observed from the graphs. First, the values of l_r for M366 are exceptionally low for heel angle equal to 15 and 20 degrees except for the forward speed of a 0.46 Froude Number value. The values of l_r are less than the value of OG at the above conditions, which implies that the lift force acts on the ship hull above the still water level. It can be mainly attributed to the geometric orientation of the ship hull at those particular conditions. For models at a larger angle of heel, a part of the lift force acts on the bottom part of the ship hull in the upward direction. In
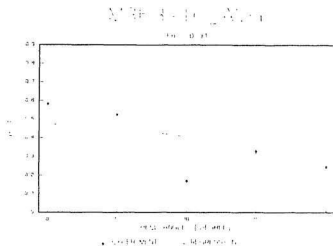
Figure 16(b) l_i/T vs. φ for M363 at Fn = 0.31
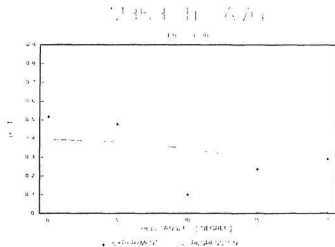
Figure 16(c) l_i/T vs. φ for M363 at Fn = 0.36
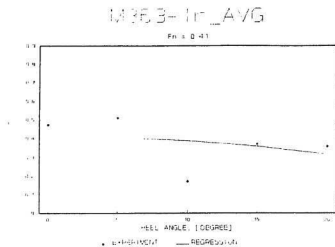
Figure 16(d) l_r/T vs. φ for M363 at Fn = 0.41
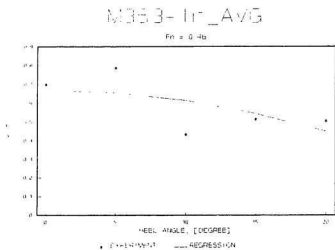
Figure 16(e) l_r/T vs. φ for M363 at Fn = 0.46
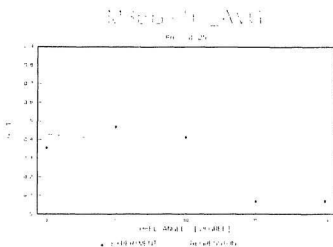
Figure 17(a) l_r/T vs. φ for M366 at Fn = 0.25
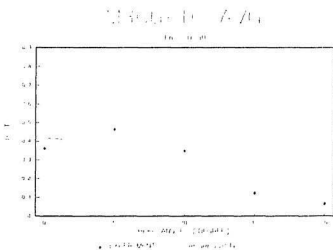
Figure 17(b) l_r/T vs. φ for M366 at Fn = 0.30
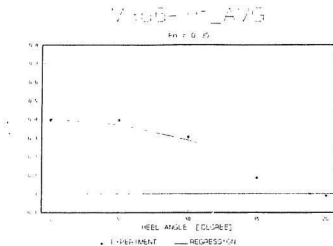
Figure 17(c) l_r/T vs. φ for M366 at Fn = 0.35
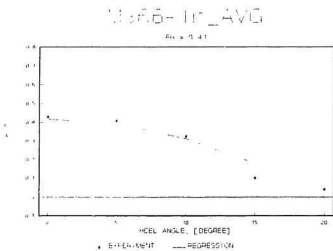
Figure 17(d) l_r/T vs. φ for M366 at Fn = 0.41
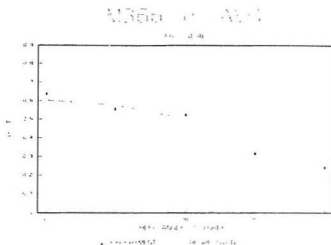
Figure 17(e) l_r/T vs. φ for M366 at Fn = 0.46

addition, the effect of the vertical force components, from sources other than dynamic lift, on the measured moment values may not be completely eliminated due to that change of geometric orientation of the ship hull. The combined effects of these upward forces may reduce the measured moment values which in turn leads to the decrease of the calculated moment arm values. Furthermore, the ship could be viewed as a three dimensional wing. The pressure distribution is non-uniform in the vertical direction, and is affected by forward speed. This may cause the lift force to act very near to the waterline. A further investigation with models free to heave and trim is needed.

The second peculiar observation is the relatively low values of l_r/T at 10 degrees heel for model M363 and M366R. Flow separation may account for this strange

51

behaviour. Besides the aforementioned reasons, a maximum experimental error of $\pm 10\%$ may also produce these peculiar results.

Since there are few previous studies in the effect of heel angle on the behaviour of center of side force acting on a moving ship hull, further investigation in this area is recommended.

4.3   Equivalent Linear Damping Coefficient

Equation (19) shows that the equivalent linear damping coefficient B_L is a function of forward speed, heel angle, coefficient β and moment arm. It is also shown in Figures 13-17 and Appendices C, D, G and H that β and l_r are functions of both forward speed and heel angle. The coefficients a_0, a_1, b_0 and b_1 of the linear plus quadratic angle dependent model were therefore plotted against Froude Number and the results are presented in Figures 18 and 19. The values of all four coefficients can be fitted into quadratic polynomials. As a result, the expressions for β and l_r/T as a function of Froude Number and φ were obtained as

$$\beta = (b_0 + b_1 \varphi^2)$$

$$= [(x_0 + x_1 Fn + x_2 Fn^2) + (y_0 + y_1 Fn + y_2 Fn^2) \varphi^2] \tag{23}$$

$$\frac{l_r}{T} = (a_0 + a_1 \varphi^2)$$

$$= [(p_0 + p_1 Fn + p_2 Fn^2) + (q_0 + q_1 Fn + q_2 Fn^2) \varphi^2] \tag{24}$$

where x_i, y_i, p_i, q_i ($i = 0,1,2$) are coefficients of the polynomials. The values of these coefficients are given in Table IV.

Figure 18(a) Coefficients b_0 and b_1 vs. Fn for M363

By comparing equations (23) and (24) to equations (20) and (21) respectively, it can be seen that the only difference between them is the presence of the φ^2 term in

53
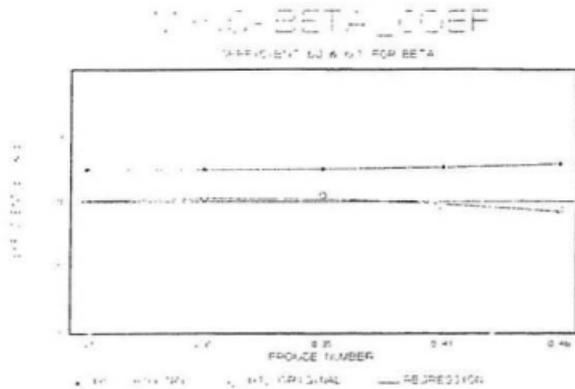
Figure 18(b) Coefficients b_0 and b_1 vs. Fn for M366
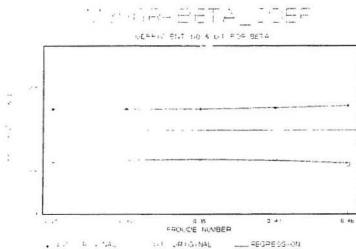
Figure 18(c) Coefficients b_0 and b_1 vs. Fn for M366R
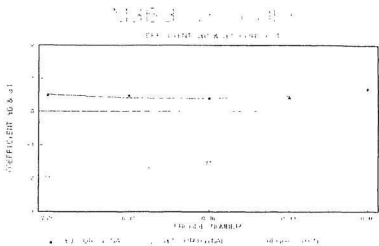
Figure 19(a) Coefficients a_0 and a_1 vs. Fn for M363
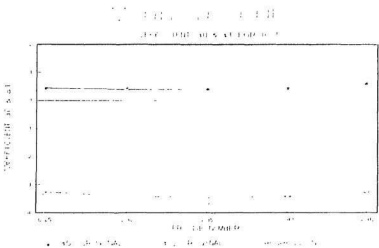
Figure 19(b) Coefficients a_0 and a_1 vs. Fn for M366
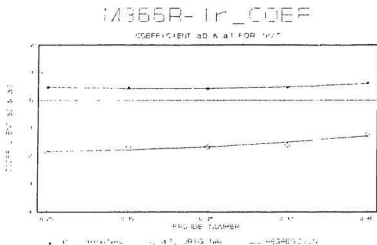
Figure 19(c) Coefficients a_0 and a_1 vs. Fn for M366R

equations (23) and (24).   Values of the regression coefficients of the constant terms b_0 and a_0 in equations (23) and (24) are very close to those of equations (20) and (21). This implies that b_0 and a_0 in equations (23) and (24) denote the upright condition terms while the φ^2 terms represent the effect of heel angle. Furthermore, the negative values of the regression coefficients of the φ^2 term indicate that the values of coefficient β and l_r will decrease with increasing heel angle.

Table IV. The values of coefficients x_i, y_i, p_i, q_i ($i=0,1,2$)

Coefficient	M363	M366	M366R
x_0	0.6041	0.3694	0.3926
x_1	-1.6560	-0.8820	-0.9791
x_2	2.4226	1.5187	1.6495
y_0	-3.0190	-0.5046	-0.8111
y_1	19.0464	3.3496	2.6563
y_2	-27.6243	-5.3026	-3.8159
p_0	2.3474	1.6338	1.6131
p_1	-11.4876	-7.6934	-7.3879
p_2	16.8696	11.8271	11.3843
q_0	-7.1389	-1.0367	-1.2639
q_1	28.0807	-13.5773	-5.1091
q_2	-34.4083	18.9604	11.0926

By substituting equations (23) and (24) into equation (19), the general expression for the equivalent linear damping coefficient B_L becomes

$$B_L = \frac{2}{\pi R^2} \rho L T V^{(2-n)} \omega^{(n-1)} [R^{(1-n)} \alpha_1 + R^{(3-n)} \alpha_2 + R^{(5-n)} \alpha_3] \qquad (25)$$

where

$$\omega = natural\ frequency$$

$$R = roll\ amplitude$$

$$\alpha_1 = e_0 \int_0^{\frac{\pi}{2}} \cos^{(1+n)} u\, du$$

$$\alpha_2 = e_1 \int_0^{\frac{\pi}{2}} \cos^{(1+n)} u \sin^2 u\, du$$

$$\alpha_3 = e_2 \int_0^{\frac{\pi}{2}} \cos^{(1+n)} u \sin^4 u\, du$$

$$e_0 = (a_0 T)^{(1+n)} b_0$$

$$e_1 = (1+n) a_1 a_0^n T^{(1+n)} b_0 + (a_0 T)^{(1+n)} b_1$$

$$e_2 = (1+n) a_1 a_0^n T^{(1+n)} b_1$$

Details of the derivation of equation (25) are given in Appendix I. A Fortran program was written to perform the computation of the equivalent linear damping coefficient B_L. A copy of the program is given in Appendix J.

Five different values of R were used to calculate the equivalent linear damping coefficient B_L. The results are shown in figures 20(a)-(c). Similar to the case of upright condition, B_l appears as a nonlinear function of Froude Number and can be separated into two distinct regions. The first region falls in the range of $0.25 \leq Fn \leq 0.36$, which B_L can be approximated as a slightly increasing linear function in the Froude

Number. In the second region, defined by Fn > 0.36, a drastic increase in the value of B_L with increasing Fn value is obtained.

B_L vs. Fn FOR MODEL M363
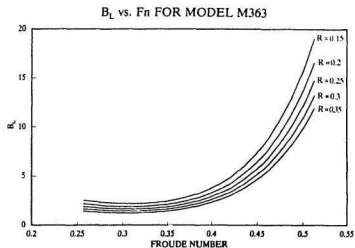
Figure 20(a) B_L vs. Fn for M363 at different R values

It can also be seen from the graphs that the larger the value of roll amplitude R used, the smaller the value for B_I. This coincides with the fact that the value of moment arm about the heel axis decreases as the heel angle increases, see Figures 16-17 and Appendix H. As mentioned before, the value of B_L is governed by the behaviour of the moment arm about heel axis, which can be seen from equation (19). Yet, the effect of R is more significant at lower speed than at higher speed.
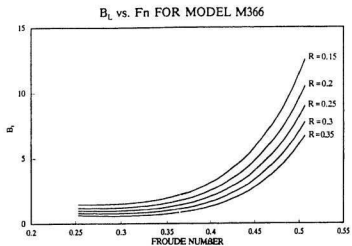
Figure 20(b) B_L vs. Fn for M366 at different R values
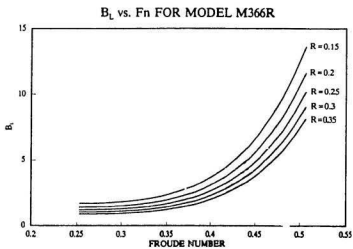
Figure 20(c) B_L vs. Fn for M366R at different R values

As in the upright condition, the contribution of the rudder to the value of B_l is more significant at low speeds than at high speeds. At a Froude Number of 0.25 and R equals to 0.35, the value of B_l is increased by about 40% with the addition of a rudder. This increase in the value of B_l drops to about 22% at a Froude Number of 0.51. At the more reasonable Froude number of 0.46, the presence of a rudder increases the value of B_l by about 33%. In addition, Figures 20(b) and 20(c) also show the effect of the value of R used on the contribution of the rudder. The graphs show that the contribution of the rudder to the damping coefficient is more significant with larger values of R. The increase in the value of B_l by the presence of a rudder at a Froude Number of 0.25 is only 16% at a value of R equal to 0.15, compared to the corresponding increase of 40% at R equal to 0.35. Among the three ship models, M363 has the largest value of equivalent linear damping coefficient. This is because it has a higher lift coefficient value than the other two ship models, see Figures 15(a)-(e) and Appendix G.

A comparison of the resulting equivalent linear damping coefficient B_l by equation (25) with Ikeda's formula will be carried out in the following chapter.

CHAPTER 5   COMPARISON OF EXPERIMENTAL RESULTS WITH IKEDA'S FORMULA

The computed equivalent linear damping coefficients from the experimental results for zero heel and non-zero heel conditions are compared with Ikeda's formula. A roll motion amplitude value of 0.35, which is equivalent to 20 degrees, is used to calculate the value of B_L. This value is chosen because it is the maximum roll amplitude within the experimental range. The results are presented in Figures 21-23. Because of the peculiar behaviour of the moment arm values at heel angles greater than 15 degrees for model M366, an amplitude value of 0.25 which is about 14 degrees is also used to determine the value of B_L and the result is shown as Figure 24. The values of B_L for non-zero heel models are less than that of the zero heel models. This is due to the fact that values of the lift moment arm about the heel axis decreases with increasing heel angle. However, both the zero heel and non-zero heel models exhibit the nonlinear relationship between the equivalent linear damping coefficient and forward speed.

Figures 21-24 also demonstrate that Ikeda's formula underestimates the equivalent linear damping coefficient for all three ship models when compared with equation (25). The discrepancy increases drastically after the Froude number has reached a value of about 0.36 due to the nonlinearity of equation (25). As can be seen in figures 21-24, the
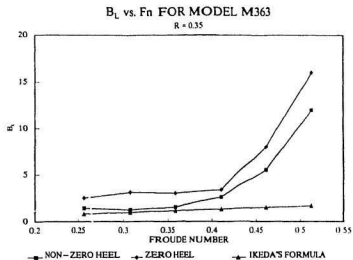
Figure 21 B_L vs. Fn for M363 with R=0.35
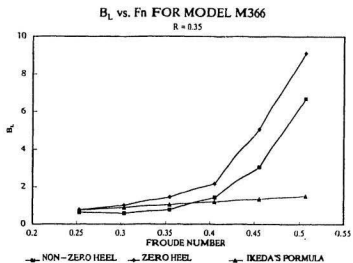
Figure 22 B_L vs. Fn for M366 with R=0.35
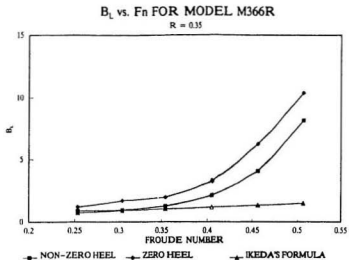
Figure 23 B_L vs. Fn for M366R with R=0.35
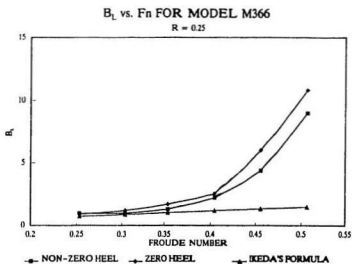
Figure 24 B_L vs. Fn for M366 with R=0.25

experimental value of B_L is a nonlinear function of the Froude number while Ikeda's formula is a linear one. This is because Ikeda assumed that the lift coefficient is a linear function of the angle of attack while the experimental results show that it is a nonlinear one. Ikeda's formula also failed to reflect the effect of forward speed on the moment arm. At a Froude number of 0.5, predicted values of B_L by Ikeda's formula are only about 14-20 % of that by equation (25). For the region of $0.25 \leq Fn \leq 0.35$, Ikeda's predictions slightly underestimate the values of B_L. Except for model M366 with an amplitude value of 0.35, Ikeda's predictions are approximately 80% of that by equation (25) in this region. For model M366 with an amplitude value of 0.35, the experimental values of B_L are about 75% of that by Ikeda's formula. At a reasonable value of Froude number of 0.46, the values of B_L by Ikeda's formula are about 30-40% of that by equation (25).

In addition, while Figure 24 shows that Ikeda's formula underestimates the value of B_L for M366 with smaller amplitude value, Figure 22 indicates that Ikeda's formula slightly overestimates the value of B_L at lower speed. The overestimation may be attributed to the round bilge ship hull characteristics of M366 since Ikeda's formula does not consider this factor. Therefore, further investigation is suggested for other ship hull forms.

Another drawback to Ikeda's formula is its inability to reflect the effect of the presence of a rudder. In contrast, this effect is taken into account in equation (25) by appropriate selection of coefficients.

It is known that the ship model sinkage increases with forward speed. When a ship moves in the water, the fluid speed on the ship hull will increase, which creates a low pressure area under the ship hull. The ship's draft increases with forward speed to balance the decreasing pressure under the ship hull. As a result, the ship's draft and OG values will alter. Both Ikeda's formula and the current experimental setup failed to address this matter. This sinkage may have effect on the measured forces acting on the model in the heeled position, while no such effect is expected for the model in the upright condition. It is suggested that the experiment be modified to allow the ship model to heave freely in future studies to remedy this problem. Zhang [1993] recommended a modification of Ikeda's formula to account for this matter. The final modification of Ikeda's formula by Zhang [1993] is given as

$$
B_L = \frac{1}{2} \rho\, LTV k_N l_o l_R [1 + 1.4\, \frac{OG_0 - (-0.8485\, C_B + 0.5032)\, Fn}{l_R} \\
+ 0.7\, \frac{(OG_0 - (-0.8485\, C_B + 0.5032)\, Fn)^2}{l_o l_R}]
$$

(26)

where OG_0 is the OG value at zero forward speed, C_B is the block coefficient of the ship model.

Generally speaking, Ikeda's formula underestimates the equivalent linear damping coefficient for all three ship models when compared with the experimental values by equation (25). In the first range of $0.25 \leq Fn \leq 0.36$, the underestimation is minor. However, in the region of $Fn > 0.36$, the underestimation becomes more and more significant.

CHAPTER 6   CONCLUSIONS

An experimental study was conducted to determine lift roll damping by measuring the lift force and moment acting on the ship hull of three ship models with different hull characteristics. The experiments were repeated with the ship models oriented in different combinations of fixed heel angles and yaw angles, and towed at various forward speeds. The four parameters, lift force, moment, lift coefficient and moment arm about the heel axis were calculated. The forward speed dependence of these parameters were studied for the ship models in both upright and heeled conditions. The equivalent linear damping coefficients were then determined and compared with Ikeda's formula. The following conclusions are reached.

1. Lift coefficient is found to be a nonlinear function of the angle of attack rather than the linear one suggested by Ikeda. It is also a nonlinear function of heel angle and forward speed.

2. Ikeda assumed the lift moment arm about the roll axis to be a constant which depends on the draft of the ship only. Experimental results show that the moment arm about the heel axis is a nonlinear function of both heel angle and forward speed.

3. Part of the lift force acting on the bottom part of the ship hull in the upward direction may attribute to the exceptionally low values of l_r at large heel angles

for model M366. The possibility of flow separation may cause the relative low values of moment arm about heel axis at 10 degrees heel for models M363 and M366R.

4. Experimental results show that the equivalent linear damping coefficient B_l is a nonlinear function of forward speed while Ikeda's formula indicates a linear relationship.

5. Ikeda's formula cannot be used as a universal prediction method for lift roll damping. At low speeds, Ikeda's formula slightly underestimates the values of B_L when compared with the experimental results. At higher speeds, the discrepancy increases. At a Froude number of 0.46, Ikeda's prediction is less than half of the experimental value.

6. The values of B_L for zero heel model are larger than the B_l values for non-zero heel model because of the decrease in lift moment arm about the heel axis with increasing heel angle.

7. The value of B_L for model M363 is higher than that of M366 due to the higher aspect ratio and thickness ratio which M363 possessed.

8. Effect of the presence of a rudder on the value of B_L is more significant at low speeds than at high speeds.

9. Ikeda's formula does not reflect the effect of the presence of a rudder.

10. Both Ikeda's formula and the current experiment failed to consider the sinkage of the ship while moving. This sinkage results in the increase of ship's draft and

decrease of the OG value. The experimental results can be improved to include this effect by allowing the ship model to heave freely.

11. The relationship between the lift moment arm and heel angle needs further study. Further investigation is also recommended on other ship hull forms.

REFERENCES

1. Abbott, I.H. and Von Doenhoff, A.E. [1959]. THEORY OF WING SECTIONS, Dover Publications, Inc., New York.

2. Abicht, W. [1975]. "On Capsizing of Ships in Regular and Irregular Seas", International Conference on Stability of Ships and Ocean Vehicles, Glasgow, C. Kuo ed.

3. Cardo, A., Francescutto, A. and Nabergoj, R. [1982]. "Technical Note on Damping Models in Free and Forced Rolling Motion", Ocean Engineering, Vol. 9, No. 2, pp. 171-179.

4. Crane, C.L., Eda, H. and Landsburg, A.C. [1989]. CONTROLLABILITY, Chapter 9 of PRINCIPLES OF NAVAL ARCHITECTURE, Vol. III, Lewis, E.V. editor, Published by the Society of Naval Architects and Marine Engineers, New Jersey.

5. Cumming, D., Haddara, M.R. and Graham, R. [1990]. "Experimental Investigation of Roll Damping Characteristics of a Destroyer Model", Proceedings of the Fourth International Conference on Stability of Ships and Ocean Vehicles, Napoli, Italy, pp. 159-166.

6. Haddara, M.R. [1984]. "A Note on the Effect of Damping Moment Form on Rolling Response", International Shipbuilding Progress, Vol. 31, No. 363, pp. 285-290.

7. Haddara, M.R. and Bennett, P. [1989]. "A Study of the Angle Dependence of Roll Damping Moment", Ocean Engineering, Vol. 16, No. 4, pp. 411-427.

8. Himeno, Y. [1981]. "Prediction of Ship Roll Damping - State of the Art", Department of Naval Architecture and Marine Engineering, University of Michigan, Report No. 239.

9. Ikeda, Y., Himeno, Y. and Tanaka, N. [1978]. "A Prediction Method for Ship Roll Damping", Report No. 00405 of Department of Naval Architecture, University of Osaka Prefecture.

10. Kerwin, J.E. [1955]. "Notes on Rolling in Longitudinal Waves", International

Shipbuilding Progress, Vol. 2, No. 16, pp. 597-614.

11.   Mandel, P. [1969].   WATER, AIR, AND INTERFACE VEHICLES,
       Massachusetts Institute of Technology, Cambridge, Mass.

12.   Schmitke, R.T. [1978]. "Ship Sway, Roll and Yaw Motions in Oblique Seas",
       Transactions of the Society of Naval Architects and Marine Engineers, Vol. 86,
       pp. 26-46.

13.   Troesch, A.W. [1981]. "Sway, Roll, and Yaw Motion Coefficients Based on a
       Forward Speed Slender-Body Theory - Part 1", Journal of Ship Research, Vol.
       25, No. 1, pp. 8-15.

14.   Watanabe, I. [1977].   "On the Effect of the Forward Velocity on the Roll
       Damping Moment", Papers of Ship Research Institute, No. 51.

15.   White, F.M. [1986]. FLUID MECHANICS, Second Edition, McGraw-Hill Book
       Company, U.S.A.

16.   Zhang, S. [1993].   "Experimental Study of the Effect of Forward Speed and
       Following Waves on Roll Damping of Fishing Vessels", M. Eng. thesis,
       Memorial University of Newfoundland, St. John's, Newfoundland, Canada.

BIBLIOGRAPHY

1. Barr, R.A. and Ankudinov, V. [1977]. "Ship Rolling, Its Prediction and Reduction Using Roll Stabilization", Marine Technology, Vol. 14, No. 1, pp. 19-41.

2. Bennett, P. [1989]. "The Angle Dependence of the Roll Damping Moment", M. Eng. thesis, Memorial University of Newfoundland, St. John's, Newfoundland, Canada.

3. Bollay, W. [1939]. "A Non-linear Wing Theory and its Application to Rectangular Wings of Small Aspect Ratio", Z. angew. Math. Mech. Bd., 19, No. 1.

4. Daoud, N.A.H. [1973]. "Force and Moments on Asymmetric and Yawed Bodies in a Free Surface", Ph. D. thesis, University of California, Berkeley, California, U.S.A..

5. Haddara, M.R. [1971]. "On the Stability of Ship Motion in Regular Oblique Waves", International Shipbuilding Progress, Vol. 18, No. 207, pp. 416-433.

6. Hoerner, S.F. and Borst, H.V. [1985]. FLUID DYNAMIC LIFT, Second Edition, Published by Mrs. L.A. Hoerner.

7. Hunter, W.S. and Joubert, P.N. [1988]. "Side Forces on a Ship's Hull", Journal of Ship Research, Vol. 32, No. 3, pp. 203-207.

8. Murray, A.B. [1950]. "The Hydrodynamics of Planing Hulls", Trans. Soc. Nav. Archit. Mar. Engrs., Vol. 58, pp. 658-692.

9. Newman, J.N. [1986]. MARINE HYDRODYNAMICS, Mit Press.

10. Yermolenko, S.D. [1967]. "Nonlinear Theory of Wings of Small Aspect Ratio", NASA TT F-10, 915.

APPENDIX A

Graphs of Lift Force Verses Froude Number

for Ship Models M363, M366 and M366R
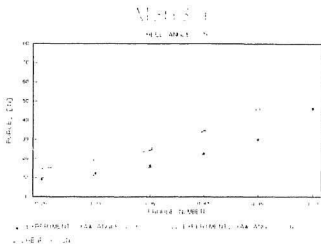
Figure A1 Force vs. Fn for M363 at $\varphi = 5^o$
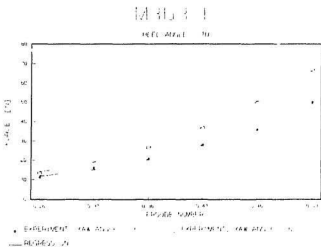
Figure A2 Force vs. Fn for M363 at $\varphi = 10^o$
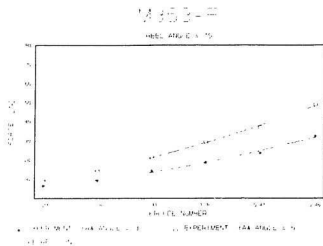
Figure A3 Force vs. Fn for M363 at $\varphi = 15°$
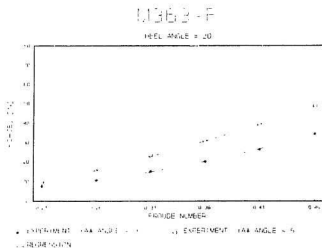
Figure A4 Force vs. Fn for M363 at $\varphi = 20°$
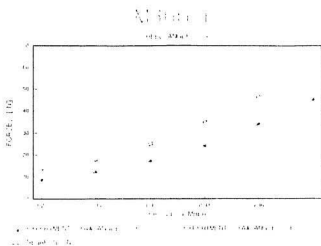
Figure A5 Force vs. Fn for M366 at $\varphi = 5°$
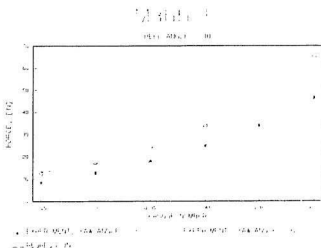
Figure A6 Force vs. Fn for M366 at $\varphi = 10°$
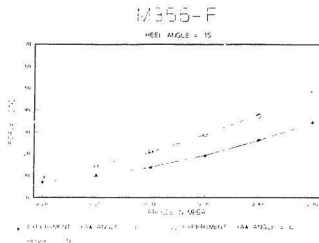
Figure A7   Force vs. Fn for M366 at $\varphi = 15^o$
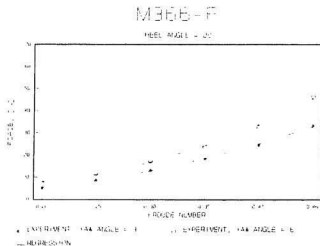
Figure A8   Force vs. Fn for M366 at $\varphi = 20^o$
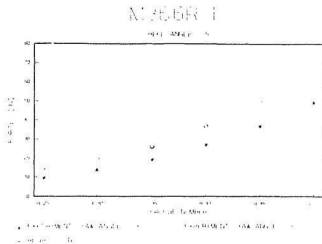
Figure A9 Force vs. Fn for M366R at $\varphi = 5°$
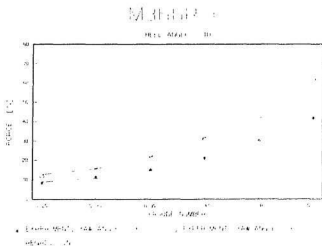
Figure A10   Force vs. Fn for M366R at $\varphi = 10°$
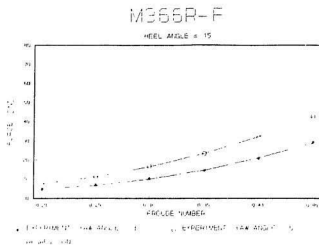
Figure A11   **Force vs. Fn for M366R at $\varphi = 15^o$**
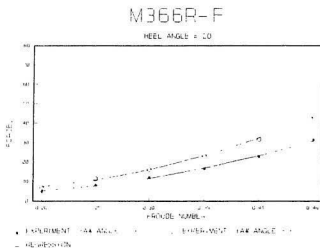
Figure A12   **Force vs. Fn for M366R at $\varphi = 20^o$**

APPENDIX B

Graphs of Moment Verses Froude Number

for Ship Models M363, M366 and M366R
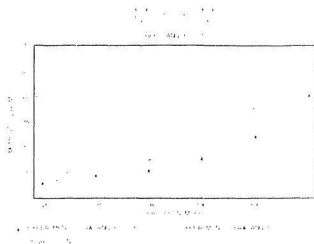
Figure B1 Moment vs. Fn for M363 at $\varphi = 5^\circ$
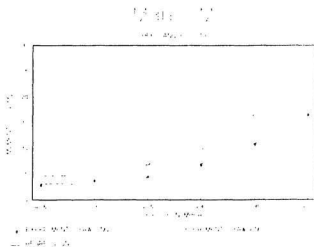
Figure B2 Moment vs. Fn for M363 at $\varphi = 10^\circ$
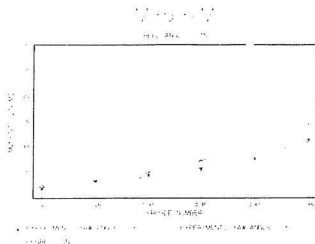
Figure B3 Moment vs. Fn for M363 at $\varphi = 15°$
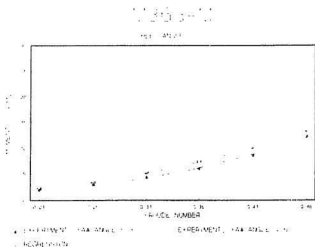
Figure B4 Moment vs. Fn for M363 at $\varphi = 20°$
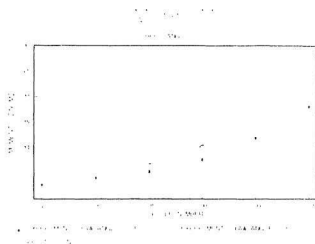
Figure B5 Moment vs. Fn for M366 at $\varphi = 5^\circ$
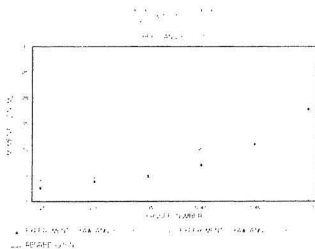
Figure B6 Moment vs. Fn for M366 at $\varphi = 10^\circ$
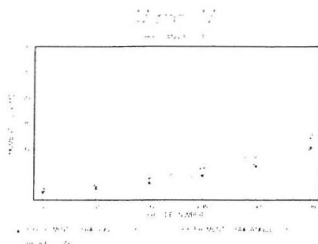
Figure B7 Moment vs. Fn for M366 at $\varphi = 15^\circ$
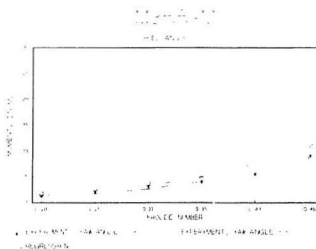
Figure B8 Moment vs. Fn for M366 at $\varphi = 20^\circ$
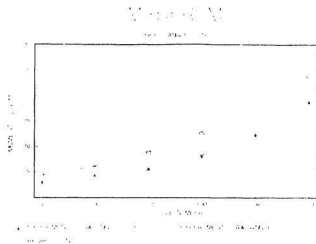
Figure B9   Moment vs. Fn for M366R at $\varphi = 5°$
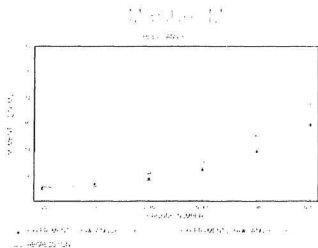
Figure B10   Moment vs. Fn for M366R at $\varphi = 10°$
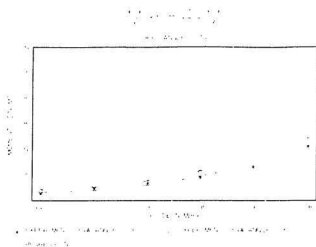
Figure B11   **Moment vs. Fn for M366R at $\varphi = 15°$**
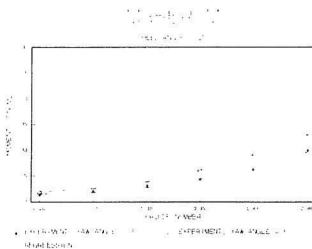
Figure B12   **Moment vs. Fn for M366R at $\varphi = 20°$**

APPENDIX C

Graphs of Coefficient β Verses Froude Number

for Ship Models M363 and M366
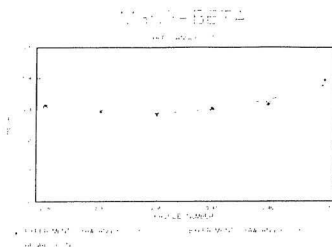
Figure C1 β vs. Fn for M363 at $\varphi = 5^\circ$
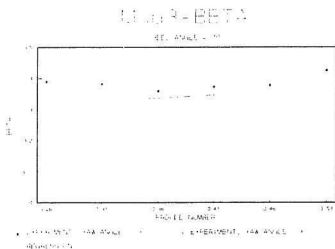
Figure C2 β vs. Fn for M363 at $\varphi = 10^\circ$
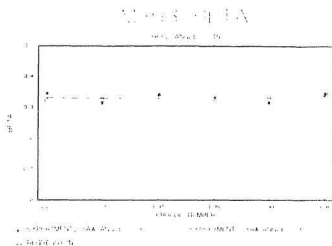
Figure C3 β vs. Fn for M363 at $\varphi = 15°$
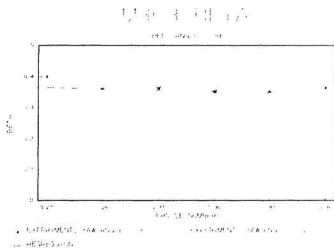
Figure C4 β vs. Fn for M363 at $\varphi = 20°$
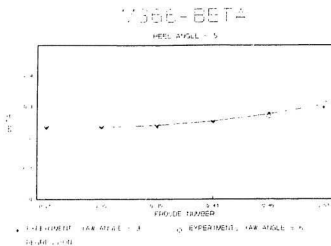
Figure C5 β vs. Fn for M366 at $\varphi = 5°$
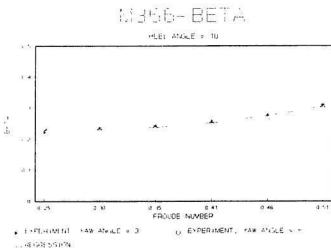
Figure C6 β vs. Fn for M366 at $\varphi = 10°$
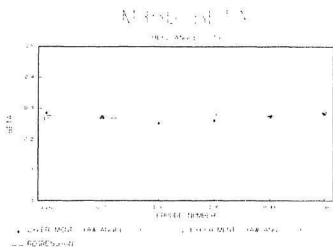
Figure C7 β vs. Fn for M366 at $\varphi = 15^{\circ}$
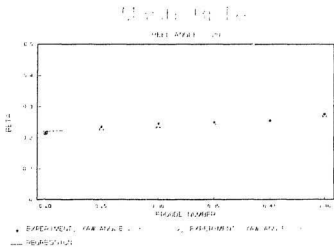
Figure C8 β vs. Fn for M366 at $\varphi = 20^{\circ}$

APPENDIX D

Graphs of Non-dimensional Moment Arm l_r/T About the Heel Axis

Verses Froude Number for Ship Models M363 and M366
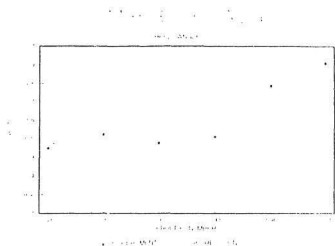
Figure D1 l_r/T vs. Fn for M363 at $\varphi = 5^o$
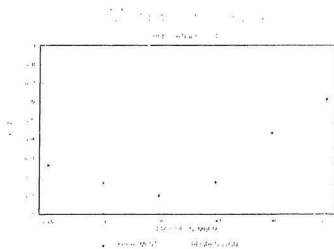
Figure D2 l_r/T vs. Fn for M363 at $\varphi = 10^o$
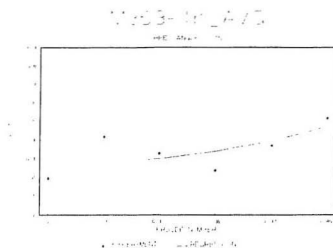
Figure D3 l_r/T vs. Fn for M363 at $\varphi = 15°$
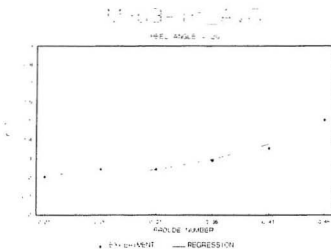
Figure D4 l_r/T vs. Fn for M363 at $\varphi = 20°$
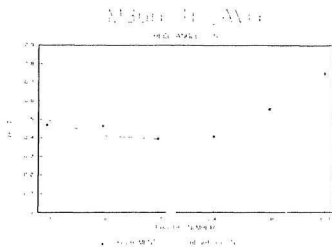
Figure D5 l_r/T vs. Fn for M366 at $\varphi = 5^o$
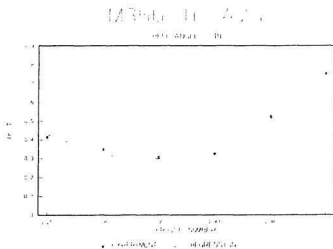
Figure D6 l_r/T vs. Fn for M366 at $\varphi = 10^o$
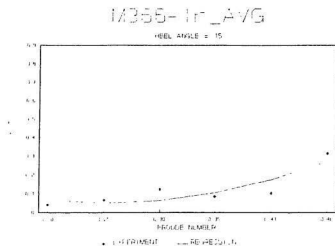
Figure D7 l_r/T **vs. Fn for M366 at** $\varphi = 15^{\circ}$
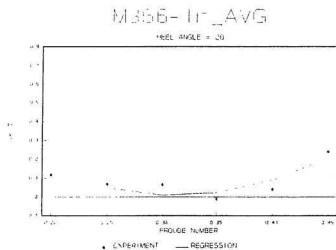
Figure D8 l_r/T **vs. Fn for M366 at** $\varphi = 20^{\circ}$

APPENDIX E

Graphs of Lift Force Verses Heel Angle

for Ship Models M363, M366 and M366R
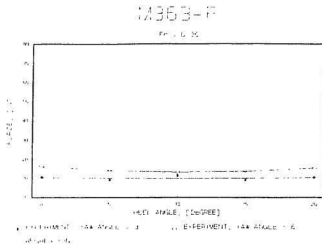
Figure E1 Force vs. φ for M363 at Fn = 0.26
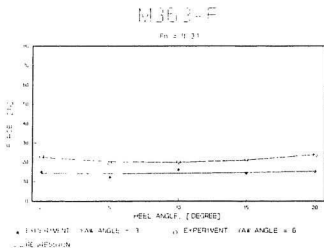

Figure E2 Force vs. φ for M363 at Fn = 0.31
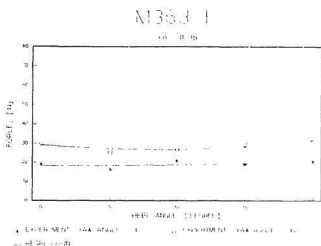
Figure E3   Force vs. φ for M363 at Fn = 0.36
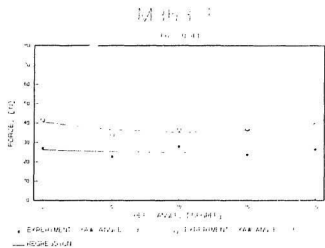
Figure E4   Force vs. φ for M363 at Fn = 0.41
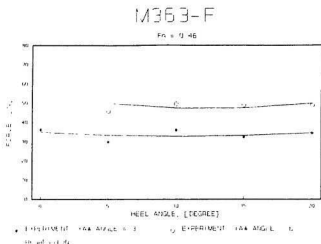
Figure E5   Force vs. φ for M363 at Fn = 0.46
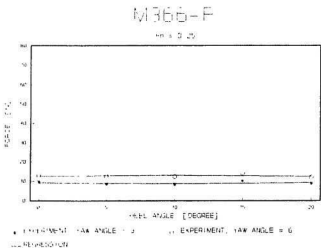
Figure E6   Force vs. φ for M366 at Fn = 0.25
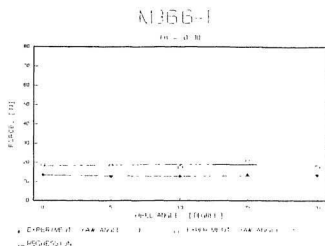
Figure E7 Force vs. φ for M366 at Fn = 0.30
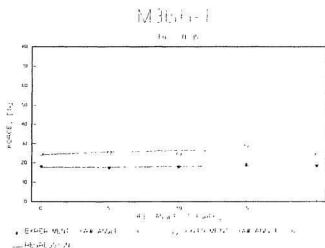
Figure E8 Force vs. φ for M366 at Fn = 0.35
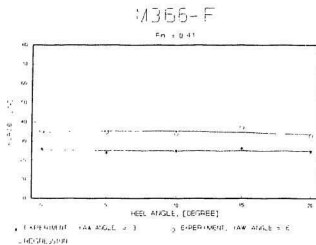
Figure E9 Force vs. φ for M366 at Fn = 0.41
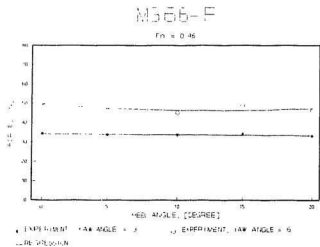
Figure E10   Force vs. φ for M366 at Fn = 0.46
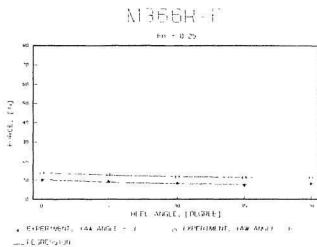
Figure E11   **Force vs. φ for M366R at Fn = 0.25**
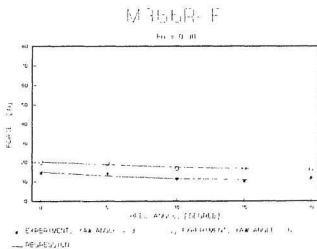
Figure E12   **Force vs. φ for M366R at Fn = 0.30**
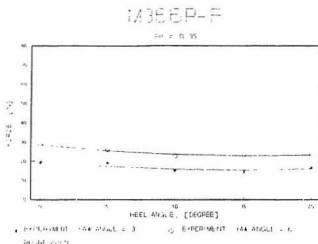
Figure E13   **Force vs. φ for M366R at Fn = 0.35**
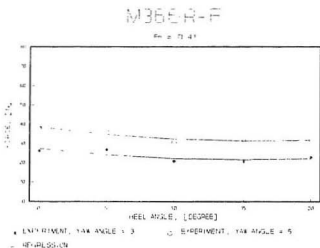
Figure E14   **Force vs. φ for M366R at Fn = 0.41**
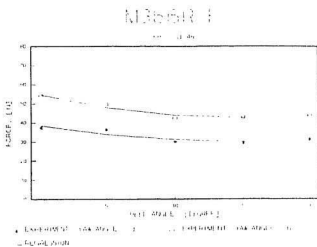
Figure E15   **Force vs. φ for M366R at Fn = 0.46**

APPENDIX F

Graphs of Moment Verses Heel Angle

for Ship Models M363, M366 and M366R
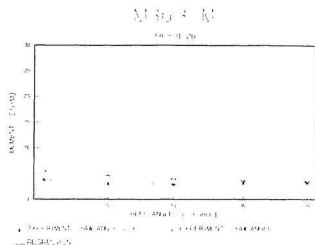
Figure F1 Moment vs. φ for M363 at Fn = 0.26
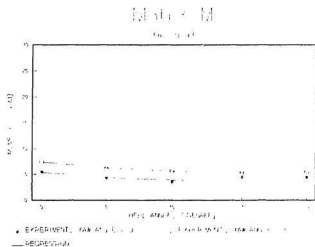
Figure F2 Moment vs. φ for M363 at Fn = 0.31
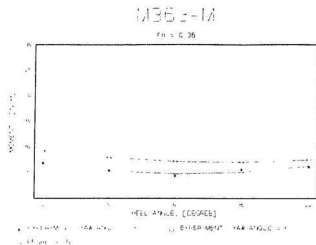
Figure F3   Moment vs. φ for M363 at Fn = 0.36
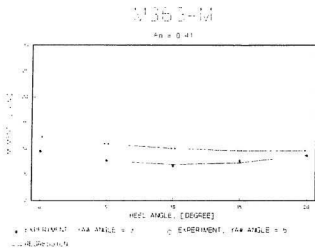
Figure F4   Moment vs. φ for M363 at Fn = 0.41
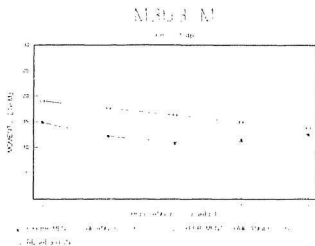
Figure F5 Moment vs. φ for M363 at Fn = 0.46
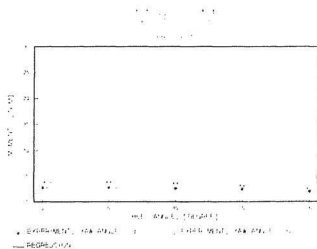

Figure F6 Moment vs. φ for M366 at Fn = 0.25
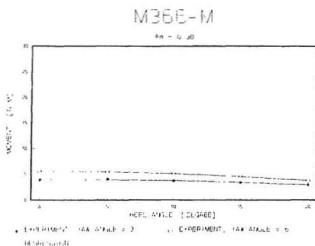
**Figure F7   Moment vs. φ for M366 at Fn = 0.30**
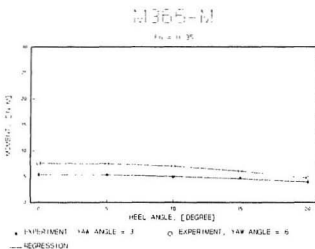
Figure F8   Moment vs. φ for M366 at Fn = 0.35
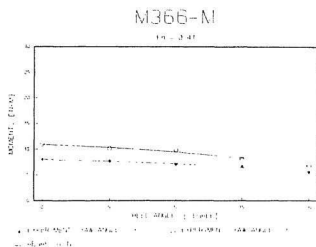
Figure F9   Moment vs. φ for M366 at Fn = 0.41
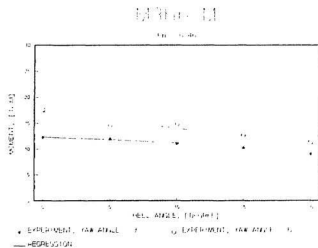
Figure F10 Moment vs. φ for M366 at Fn = 0.46
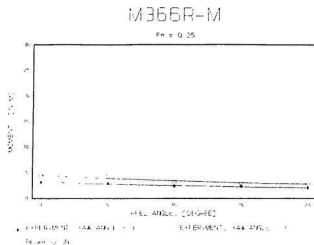
Figure F11 Moment vs. φ for M366R at Fn = 0.25
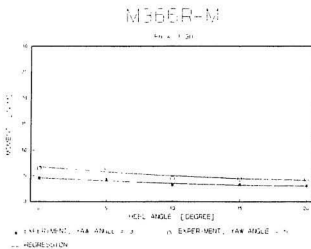

Figure F12 Moment vs. φ for M366R at Fn = 0.30
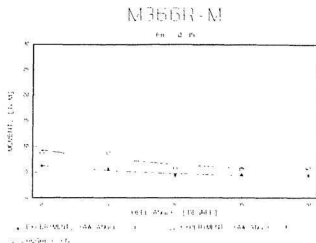
Figure F13 Moment vs. φ for M366R at Fn = 0.35
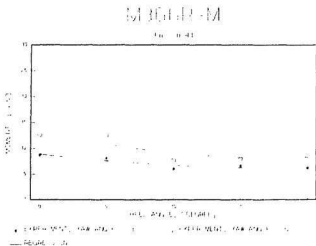
Figure F14 Moment vs. φ for M366R at Fn = 0.41
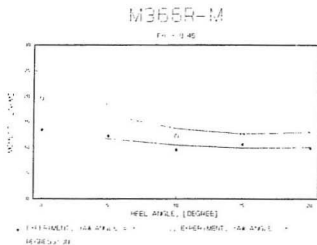
**Figure F15 Moment vs. φfor M366R at Fn = 0.46**

Graphs of Coefficient β Verses Heel Angle

for Ship Models M363 and M366
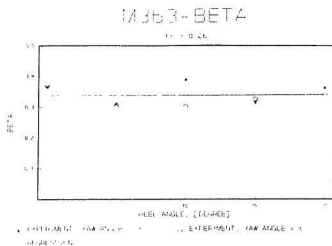
Figure G1 β vs. φ for M363 at Fn = 0.26
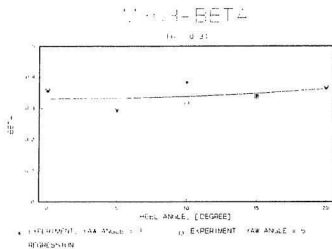
Figure G2 β vs. φ for M363 at Fn = 0.31
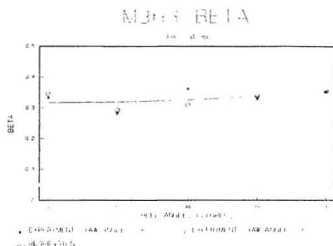
Figure G3 β vs. φ for M363 at Fn = 0.36
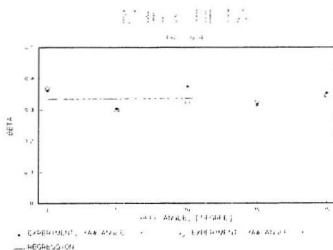
Figure G4 β vs. φ for M363 at Fn = 0.41
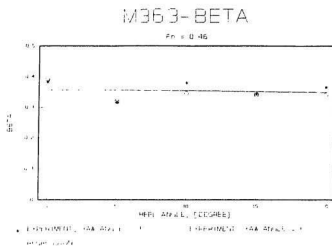
Figure G5 β vs. φ for M363 at Fn = 0.46
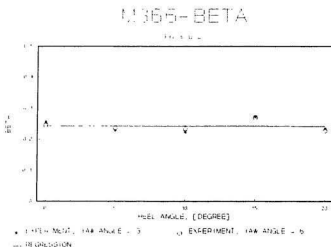
Figure G6 β vs. φ for M366 at Fn = 0.25
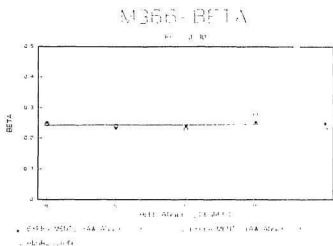
Figure G7 β vs. φ for M366 at Fn = 0.30
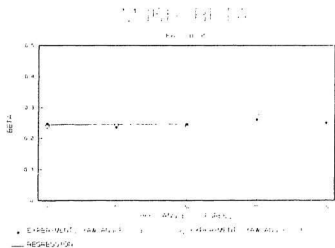

Figure G8 β vs. φ for M366 at Fn = 0.35
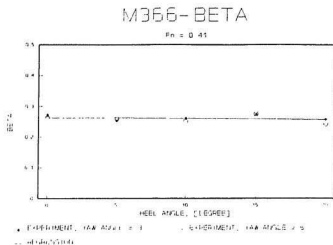
Figure G9 β vs. φ for M366 at Fn = 0.41
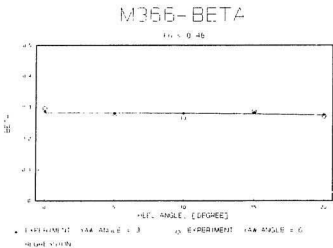
Figure G10 β vs. φ for M366 at Fn = 0.46

APPENDIX H

Graphs of Non-dimensional Moment Arm l_r/T About the Heel Axis

Verses Heel Angle for Ship Model M366R
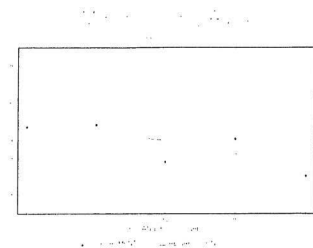
Figure H1 l_r/T vs. φ for M366R at Fn = 0.25
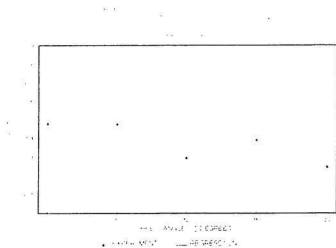
Figure H2 l_r/T vs. φ for M366R at Fn = 0.30
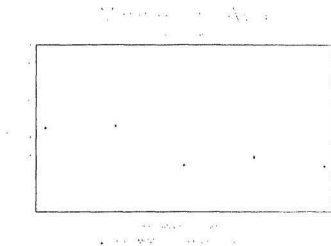
Figure H3 I_r/T vs. φ for M366R at Fn = 0.35
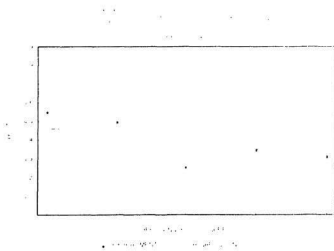
Figure H4 I_r/T vs. φ for M366R at Fn = 0.41
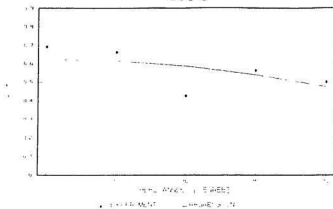
Figure II5 l_t/T vs. φ for M366R at Fn = 0.46

APPENDIX I

Derivation of Equivalent Linear Damping Coefficient B_L

Derivation of Equivalent Linear Damping Coefficient B_L

$$\psi = \frac{l_r \dot{\psi}}{V}$$

$$\beta = b_0 + b_1 \varphi^2$$

$$l_r = a_0 + a_1 \varphi^2$$

$$F = \frac{1}{2} \rho V^2 LT \beta \psi^n$$

$$M = F \cdot l_r$$

$$= \frac{1}{2} \rho V^{(2-n)} LT \beta l_r^{(1+n)} \dot{\psi}^n$$

$$\left(\frac{l_r}{T}\right)^{(1+n)} = (a_0 + a_1 \varphi^2)^{1+n}$$

$$= a_0^{(1+n)} \left[1 + \frac{a_1}{a_0} \varphi^2\right]^{1+n}$$

$$= a_0^{(1+n)} \left[1 + (1+n)\frac{a_1}{a_0}\varphi^2 + \frac{n(1+n)}{2}\left(\frac{a_1}{a_2}\right)^2 \varphi^4 + \cdots\right]$$

$$\approx a_0^{(1+n)} \left[1 + (1+n)\frac{a_1}{a_0}\varphi^2\right]$$

$$l_r^{(1+n)} = d_0 + d_1 \varphi^2$$

where $d_0 = (a_0 T)^{1+n}$ and $d_1 = (1+n) a_1 a_0^n T^{1+n}$

$$l_r^{(1-n)}\beta = e_0 + e_1 \varphi^2 + e_2 \varphi^4$$

$$where \quad e_0 = b_0 d_0$$
$$e_1 = d_1 b_0 + d_0 b_1$$
$$e_2 = d_1 b_1$$

$$\int_0^R M d\varphi = \int_0^R B_L \dot{\varphi} \, d\varphi$$

$$Let \quad \varphi = R \sin\omega t$$
$$\dot{\varphi} = R\omega \cos\omega t$$
$$d\varphi = R\omega \cos\omega t \, dt$$
$$\varphi = R \;\rightarrow\; t = \frac{\pi}{2\omega}$$

R. H. S.

$$\int_0^R B_L \dot{\varphi} \, d\varphi = B_L \int_0^{\frac{\pi}{2\omega}} R\omega \cos\omega t \, R \cos\omega t \, dt$$

$$= B_L R^2 \omega^2 \int_0^{\frac{\pi}{2\omega}} \cos^2\omega t \, dt$$

$$= \frac{\pi}{4} \omega R^2 B_L$$

L. H. S.

$$\int_0^R M d\varphi = \int_0^{\frac{\pi}{2\omega}} \frac{1}{2} \rho \, V^{(2-n)} L T (R\omega \cos \omega t)^n \times$$

$$[e_0 + e_1 R^2 \sin^2 \omega t + e_2 R^4 \sin^4 \omega t] R\omega \cos \omega t \, dt$$

$$= \frac{1}{2} \rho \, V^{(2-n)} L T (R\omega)^{(1+n)} e_0 \int_0^{\frac{\pi}{2\omega}} \cos^{(1+n)} \omega t \, dt$$

$$+ \frac{1}{2} \rho \, V^{(2-n)} L T R^{(3+n)} \omega^{(1+n)} e_1 \int_0^{\frac{\pi}{2\omega}} \cos^{(1+n)} \omega t \sin^2 \omega t \, dt$$

$$+ \frac{1}{2} \rho \, V^{(2-n)} L T R^{(5+n)} \omega^{(1+n)} e_2 \int_0^{\frac{\pi}{2\omega}} \cos^{(1+n)} \omega t \sin^4 \omega t \, dt$$

$$= \alpha_1 (R\omega)^{(1+n)} + \alpha_2 R^{(3+n)} \omega^{(1+n)} + \alpha_3 R^{(5+n)} \omega^{(1+n)}$$

$$\frac{\pi}{4} \omega R^2 B_L = \alpha_1 (R\omega)^{(1+n)} + \alpha_2 R^{(3+n)} \omega^{(1+n)} + \alpha_3 R^{(5+n)} \omega^{(1+n)}$$

$$B_L = \frac{2}{\pi R^2} \rho \, L T V^{(2-n)} \omega^{(n-1)} [R^{(1+n)} \alpha_1 + R^{(3+n)} \alpha_2 + R^{(5+n)} \alpha_3]$$

where

$$\alpha_1 = e_0 \int_0^{\frac{\pi}{2}} \cos^{(1+n)} u \, du$$

$$\alpha_2 = e_1 \int_0^{\frac{\pi}{2}} \cos^{(1+n)} u \sin^2 u \, du$$

$$\alpha_3 = e_2 \int_0^{\frac{\pi}{2}} \cos^{(1+n)} u \sin^4 u \, du$$

APPENDIX J

Listing of Fortran Program: BLIFT.FOR

```
C      BLIFT.FOR
C      This is a VAX-FORTRAN program to calculate the equivalent
C      linear damping coefficient for lift roll damping.
C
C      Kirk Sing-Keung Leung
C      November, 1992, Engineering, M.U.N.

       REAL P0,P1,P2,Q0,Q1,Q2,X0,X1,X2,Y0,Y1,Y2
       REAL A0,A1,B0,B1,C0,C1,E0,E1,E2,ALPHA1,ALPHA2,ALPHA3
       REAL T,DT,OMEGA,PI,SUM1,SUM2,SUM3,R,N,Z
       REAL DEN,L,D,U(100),BL(100),FN(100)

       CHARACTER*15 FILENAME, FNAME, MODEL

       PRINT*, 'TYPE INPUT FILENAME'
       READ 50, FILENAME
50     FORMAT (A15)
       PRINT*, 'TYPE OUTPUT FILENAME'
       READ 55, FNAME
55     FORMAT (A15)

       OPEN (5, FILE = FILENAME, STATUS = 'OLD')
       OPEN (10, FILE = FNAME, STATUS = 'NEW')

C      L=LENGTH AT WATERLINE, D=DRAFT, C OMEGA=NATURAL
FREQUENCY OF SHIP,
C      N=EXPONENT IN THE LIFT COEFFICIENT EQUATION,
C      R=MAXIMUM ROLL AMPLITUDE, DEN=WATER DENSITY,
C      U=FORWARD SPEED,
C      P0,P1,P2,Q0,Q1,Q2,X0,X1,X2,Y0,Y1,Y2 ARE REGRESSION
C      COEFFICIENTS, FN=FROUDE NUMBER,
C      BL=EQUIVALENT LINEAR DAMPING COEFFICIENT
C      FOR LIFT ROLL DAMPING.


       READ (5,100), L, D, OMEGA, N, R
100    FORMAT (5F10.6)
       READ (5,110), P0, P1, P2, Q0, Q1, Q2
       READ (5,110), X0, X1, X2, Y0, Y1, Y2
110    FORMAT (6F10.6)

       PI = 3.14159
```

131

```
       DEN = 1000.0
       T = 0.0
       DT = 0.00001
       SUM1 = 0.0
       SUM2 = 0.0
       SUM3 = 0.0


       DO WHILE ((T+DT) .LT. (PI/2))

       SUM1 = SUM1 + (F1(N,T) + F1(N,T+DT))*DT/2
       SUM2 = SUM2 + (F2(N,T) + F2(N,T+DT))*DT/2
       SUM3 = SUM3 + (F3(N,T) + F3(N,T+DT))*DT/2
       T = T + DT

       ENDDO

C      DETERMINE THE VALUES OF THE INTEGRALS
       WRITE (10,*) 'SUM1 =', SUM1
       WRITE (10,*) 'SUM2 =', SUM2
       WRITE (10,*) 'SUM3 =', SUM3
       WRITE (10,*)
130    FORMAT (5F10.6)

       WRITE (10,150) 'SPEED', 'FN', 'BL'
150    FORMAT (3A10)

       U(1) = 0.1

       DO I = 1,50

       FN(I) = U(I)/SQRT(9.81*L)
       Z = DEN*L*D*U(I)**(2-N)*OMEGA**N

       A0 = P0 + P1*FN(I) + P2*FN(I)**2
       A1 = Q0 + Q1*FN(I) + Q2*FN(I)**2
       B0 = X0 + X1*FN(I) + X2*FN(I)**2
       B1 = Y0 + Y1*FN(I) + Y2*FN(I)**2
       C0 = (A0*D)**(1+N)
       C1 = (1+N)*A1*A0**N*D**(1+N)
       E0 = B0*C0
       E1 = C1*B0 + C0*B1
```

132

```
      E2 = C1*B1
      ALPHA1 = E0 * SUM1
      ALPHA2 = E1 * SUM2
      ALPHA3 = E2 * SUM3

      BL(I) = 2*Z/(PI*OMEGA*R**2)*(R**(1+N)*ALPHA1
   &            + R**(3+N)*ALPHA2 + R**(5+N)*ALPHA3)

      WRITE (10,200) U(I), FN(I), BL(I)
200   FORMAT (3F10.4)

      U(I+1) = U(I) + 0.05

      ENDDO

      CLOSE (5)
      CLOSE (10)

      END


      FUNCTION F1(N,T)
         REAL N
         F1 = (COS(T))**(1+N)
         RETURN
      END

      FUNCTION F2(N,T)
         REAL N
         F2 = (COS(T))**(1+N)*(SIN(T))**2
         RETURN
      END

      FUNCTION F3(N,T)
         REAL N
         F3 = (COS(T))**(1+N)*(SIN(T))**4
         RETURN
      END
```